Climate impact of contrailscirrus from hydrogen combustion aircraft

Susanne M. Pettersson[1], Christian Azar[1], and Daniel J.A. Johansson[1]

[1]Department of Space, Earth and Environment, Chalmers University of Technology, Maskingränd 2, 412 58 Gothenburg, Sweden.

Correspondence: Susanne M. Pettersson (susannep@chalmers.se)

Abstract. ~~To mitigate~~ One possibility for reducing the climate impact of aviation ~~, combustion of hydrogen as a fuel is one possible future pathway~~is to transition to aircraft powered by hydrogen combustion. Hydrogen combustion leads to zero ~~carbon emissions in the exhaust , representing a~~ CO_2 exhaust emissions and represents a potential major step toward ~~climate neutrality~~reduced climate impact, although the non-CO_2 effects ~~, primary contrail cirrus~~(primarily contrail cirrus) remain uncertain. In this study, we simulate the climate impact, in terms of energy forcing, of contrail cirrus from hydrogen combustion aviation, using a modified version of the Contrail Cirrus Prediction model (CoCiP).

~~Without~~ With no soot in the exhaust~~from hydrogen combustion~~, contrail ice particles ~~instead~~ mainly form on ambient aerosols entrained into the plume and on lubrication oil droplets in the exhaust. The formation of ice particles ~~are~~ is modelled using an emulator developed from a theoretically based microphysical contrail formation model.

Following the Schmidt Applemann criterion, hydrogen combustion enables contrail formation at lower altitudes and higher temperatures than fossil jet fuel. However, we find a significant reduction in contrail energy forcing. This result holds across a wide range of assumptions, ~~including different oil particle size distributions and properties,~~ with a global average reduction of about ~~70~~66% using our base case assumptions on ambient aerosols, lubrication oil properties, droplet size distribution, emission index and energy efficiency of hydrogen aircraft. We conclude that hydrogen aircraft not only eliminate~~s~~ CO_2 emissions in the exhaust, but may also ~~substantially~~ reduce the climate impact of contrail cirrus, ~~although the reduction and magnitude depend~~ depending on engine design for lubrication oil handling. However, we acknowledge that the modelling approach has limitations and uncertainties. Before firm conclusions can be drawn about the contrail cirrus effects of hydrogen-combustion aircraft, further studies are needed. These should include more realistic hydrogen aircraft models, alternative meteorological and microphysical models, analysis of real-world flight patterns and measurement data.

1 Introduction

Contrails are ~~artificial~~ artificially induced ice clouds that can form behind aircraft (Schumann, 1996). They are initially line-shaped but ~~can~~ under certain conditions, ~~if~~ when the ambient air is humid enough, they can persist and evolve into more naturally shaped clouds. Such ~~evolved~~ contrails are referred to as contrail cirrus. As clouds, contrail cirrus affect the earth's radiative balance by reflecting incoming sunlight and trapping outgoing infrared radiation (Yang et al., 2010). Depending on a range of factors, such as the time of day, ~~the~~ prevalence of natural clouds and surface albedo, contrail cirrus can ~~either act~~ act as either net cooling or net warming. Estimates of the effective radiative forcing of global aviation show that the warming effect dominates (Lee et al., 2021). Although contrail cirrus are short-lived ~~, on the order of~~ (hours, maybe a day), their current contribution to ~~aviation~~ the overall effective radiative forcing (ERF) of aviation is estimated to ~~two thirds~~ at a little over half of the total aviation ERF, albeit with a large uncertainty (Lee et al., 2021). ~~Because of aviations valuable contribution of connecting the globe but significant contribution to climate change with approximately 3.5% of global anthropogenic climate forcing (Lee et al., 2021),~~ For that reason, it is important to map out possible routes for contrail mitigation~~are important to map out. Rerouting aircraft around contrail forming regions (Kölker et al., 2024; Rosenow and Fricke, 2018)and .~~ . Rerouting flights around contrail-forming regions (Kölker et al., 2024; Rosenow and Fricke, 2018), improved engines and the strategic usage of low aromatic fuels (Teoh et al., 2022b; Quante et al., 2024) have been suggested as possible options.

The magnitude of ~~contrail cirrus~~ the radiative forcing (RF) ~~, in addition to the above mentioned circumstances, depend~~ from contrail cirrus depends on the properties of the contrail cirrus. ~~A~~ In addition to the factors mentioned above, a higher density of ice particles ~~(all else equal)~~ increases the contrail lifetime and optical depth (Lewellen et al., 2014; Kärcher, 2016). ~~The~~ In turn, the density of ice particles ~~in turn depends on particle number and their properties at the contrail's formation~~ depends on the number and properties of the particles present when the contrail is formed (Kärcher, 2016; Yu et al., 2024). Reducing ~~particle number~~ the number of particles in the exhaust is suggested as a contrail cirrus mitigation strategy in itself~~, but~~ . However, it also comes as a co-benefit of ~~a transition to hydrogen fuel~~ transitioning to hydrogen-fuelled aircraft. Hence, hydrogen combustion, besides having no exhaust CO_2 emissions, might also be beneficial because of its decreased number of ~~particles in the exhaust . A~~ exhaust particles. One hypothesis is that the lack of soot and other ~~fossil jet fuel related~~ fossil-jet-fuel-related particles in the exhaust of hydrogen aircraft will reduce the ~~ability of ice particle formation leading to less contrails and a reduced need for rerouting with extra fuel costs~~number of formed ice particles and consequently reduce the need for other contrail mitigation measures such as flight rerouting (which causes extra fuel use).

~~However, there is uncertainty whether the lack of soot in hydrogen aircraft exhaust will lead to a reduction~~ On the other hand, hydrogen combustion is still expected to lead to some production of ice particles ~~or not. Although lacking in soot and other volatile particle matter/substances such as chemi-ions and sulfates, the hydrogen exhaust contains additional water vapour that will increase the conditions over which contrails can form. The extra water vapour might also increase the amount of ice particles that can form from the particles still present and thereby~~ and contrail formation since ambient aerosols, NO_x and lubrication oil droplets can act as condensation nuclei. Furthermore, the higher water vapour emissions from hydrogen combustion, relative to kerosene on per unit energy basis, increase both the likelihood of particle activation as condensation nuclei and the likelihood that the Schmidt–Appleman criterion is satisfied. The latter implies that contrails are expected to form over a larger area for hydrogen than for kerosene. Together, these effects may increase both the occurrence and energy forcing of contrail cirrus (Schumann, 1996). No results ~~from measurement campaigns on~~ of campaigns to measure the contrail cirrus of ~~hydrogen fuelled~~ hydrogen-fuelled aircraft have been published yet (DLR, 2025). However, several measurement campaigns testing blends of conventional jet and ~~Sustainable Aviation Fuels~~ sustainable aviation fuels (SAFs) ~~to different degree find~~ at different ratios have found a reduced number of ice particles ~~(Voigt et al., 2021) because of the~~ following a reduction in soot particles (due to reduced aromatics in the fuel) (Moore et al., 2017; Durdina et al., 2021; Zhang et al., 2022). But with even lower soot emissions than (Voigt et al., 2021; Moore et al., 2017; Durdina et al., 2021; Zhang et al., 2022). At soot emissions even lower than those measured in these campaigns (in the order of the order of $< 10^{13}$) there are indications of an increase in ice particles (kg fuel)$^{-1}$), ice particle number concentrations may increase at low temperatures due to the activation of other ultrafine particles in the exhaust (Kärcher and Yu, 2009; Yu et al., 2024)such as volatile particles (approximately radii . These may include volatile particles with approximate radii of < 5 nm) composed , consisting of condensable sulfur and organics mainly forming species and organic species formed primarily on chemi-ions(Yu and Turco, 1997; Yu et al., 1999; Kärcher et al., 2000) but including homogeneous lubrication oil droplets relevant for hydrogen combustion. Models are now being developed to capture this increase in ice particle formation due to ultrafine particles but the uncertainty is still large. , as well as homogeneously formed organic species such as lubrication oil (Yu and Turco, 1997; Yu et al., 1999; Kärcher et al., 2000; Voigt et al., 2026 .

In a A simulation study of contrail formation with hydrogen fuel the loss of soot is shown to, for aircraft powered by hydrogen combustion showed that under most circumstances, significantly reduce the amount of ice-particles the absence of soot and other fossil-jet-fuel-related particles significantly reduces the number of ice particles formed in a three seconds old plume in comparison to three-second-old plume compared to aircraft powered by fossil jet fuel (Bier et al., 2024). The circumstances conditions under which this does not hold is when are when ambient temperatures are high, near the critical threshold of contrail formation for jetfossil jet fuel, or even higher where only contrails from hydrogen are possibleaircraft can form. This simulation lets the ice particles form solely study only covers ice particle formation on ambient aerosols. It However, it has been recognised , however, that lubrication oil still present in the exhaust of hydrogen aircraft might contribute to ice particle formation in the absence of soot and other fossil-jet-fuel-related particles (Bier et al., 2024; Yu et al., 2024). Soot does not readily act as condensation nuclei a condensation nucleus for water droplets, lubrication oil droplets even less so, although they can under the right . Lubrication oil droplets are even less likely to do so, but may, nevertheless, act as condensation nuclei under suitable conditions (Ponsonby et al., 2024; Lambe et al., 2011). The When compared to the available water vapour in fossil jet fuel exhaust, the additional water vapour in the hydrogen exhaust might be enough to activate lubrication oil to form water droplets.

This study provides the first investigation of the combined effects of additional water vapour from hydrogen combustion and the potential will increase the chance of lubrication oil aerosols acting as condensation nuclei. The number of ice particles formed on ambient aerosols and lubrication oil in hydrogen combustion has been investigated in one previous study (Zink et al., 2025b) . Under certain conditions, such as a high oil emission index and small oil droplets, hydrogen combustion was found to produce more ice particles than kerosene combustion, regardless of whether lubrication oil was included in the kerosene case. This demonstrates the potential importance of lubrication oil and ambient aerosols to serve as ice nuclei in contrail formationand their radiative impact from hydrogen-powered aircraft.

The role of lubrication oil and ambient aerosols as ice nuclei is unfortunately associated with large uncertainties. For the characterisation uncertain. All published studies reporting measurements of lubrication oil in aircraft exhausts all studies published exhaust have been conducted on conventionalaircraft i.e. kerosene driven craft. Large , fossil-jet-fuel-powered aircraft. Major uncertainties stem from the fact that lubrication oil can ~~be both~~ either be vented outside the main exhaust stream or be emitted or leaked out in the exhaust at high temperatures. This leads to large differences in aerosol oil size distributions, ~~since~~ as oil is a volatile substance. In addition to uncertainties in ~~size-distribution lubrication oils' readiness~~ size distribution, the degree of readiness of lubrication oil to act as condensation nuclei is uncertain (Lambe et al., 2011). Further~~uncertainties can be found~~ , there are major uncertainties regarding the amount of lubrication oil emitted~~depending on~~ , depending on such things as oil and engine types (Yu et al., 2010; Timko et al., 2014; Decker et al., 2024).

The ~~designator ambient aerosols~~term "ambient aerosols" covers all types of particles suspended in the atmosphere. ~~Therefore~~ Consequently, there is a ~~large span~~ considerable range of particle types, sizes and properties included ~~in this category leading to large~~ among ambient aerosols, leading to major variability and uncertainties in ~~ambient aerosol~~ their characterisation (Raes et al., 2000; Clarke and Kapustin, 2002; Minikin et al., 2003)~~(, hermann, brock, voigt - kolla upp). Ambient aerosols vary in their spatial distributions, size distributions and chemical properties, a trait found in both observation campaigns (Clarke and Kapustin, 2002; Minikin et al., 2003) and emphasized in modelling of aerosol physics~~ , which has also been emphasised in the modelling of ambient aerosols in climate models (Stier et al., 2005; Kaiser et al., 2019).

~~Despite the large uncertainties and variability in both ambient aerosols' number concentration and composition and in the specifications of lubrication oil, we aim in this study to map~~ The aim of this study is to simulate the contrail cirrus climate impact of hydrogen combustion for a large set of plausible assumptions. In ~~this way we can narrow down the space of possible contrail contribution from hydrogen aircraft~~particular, the focus is on the contribution of lubrication oil emissions to contrail energy forcing (EF). We estimate ice particle numbers generated with ambient aerosols and lubrication oil as condensation nuclei. We then use this to simulate contrail cirrus formation and evolution on relevant flight levels on a global grid under realistic meteorological conditions and estimate their energy forcing. We also estimate contrail formation and EF from conventional fossil jet fuel aviation so as to enable a comparison between the two. Thus, we may give an indication of plausible contrail cirrus climate effects for hydrogen aircraft relative to that for prevailing fossil jet fuel aircraft. In addition~~we can contribute with~~ , we may contribute insights to guide the future development of hydrogen engines to avoid designs that ~~can lead to a large contrail impact~~may lead to major contrail cirrus climate impacts.

To investigate contrail ~~formation,~~ cirrus formation, plus the evolution and energy forcing from hydrogen aircraft, we use the Contrail Cirrus Prediction model (CoCiP) (Schumann, 2012)~~. CoCiP in its original formulation forms ice particles~~ , as implemented in pycontrails (Shapiro et al., 2023). CoCiP models ice particle formation solely on soot emissions (or defaults to 10^{13}(kg fuel)$^{-1}$, as a way of accounting for background ambient aerosols if the soot emissions given are lower). We modify the functions of ~~the model~~ CoCiP covering ice particle activation to explicitly include ice particles formed on lubrication oil and ambient aerosols. Given atmospheric conditions, oil emission index and oil properties~~the newly developed functions estimate the amount~~ , we use activation emulators developed in the paper to estimate the number of formed ice particles~~to initiate the contrail cirrus simulation in CoCiP for estimating radiative implications. The amount of~~ . These emulators are based on the theoretical model developed by Kärcher et al. and used to determine the amount of lubrication oil and ambient aerosols activated to ~~ice particles is based on the theoretical model put forward by Kärcher et. al~~ form ice particles (Kärcher et al., 2015). This model was originally formulated for soot and ambient aerosols but offers an approach ~~of extending~~ that extends to other types of particles, provided their characteristics are given. The number of ice particles obtained from the emulators initiate the contrail cirrus simulation in CoCiP which is subsequently used to estimate energy forcing.

2 Theory

~~A thermodynamic criterion for contrail formation, termed the~~ The Schmidt-Appleman Criterion (SAC)~~after its founders~~, a thermodynamic criterion for contrail formation named after its creators, dates back to the 1940s (Schumann, 1996). It depends on both ambient conditions and fuel exhaust properties. ~~Intuitively~~As such, the criterion requires ~~that the hot exhaust gas from the aircraft engines at some point during its cooling and mixing with ambient air becomes~~ the cooling plume to become supersaturated with respect to water ~~. The~~ at some point. This supersaturation enables the formation of water droplets~~which will~~ , which may subsequently freeze to form the contrail. The so-called mixing line of ~~the~~ an exhaust plume, tracing its temperature (T) and partial water vapour pressure (p_w) over time, can be approximated as linear in T-p_w space (excluding a brief non-linear phase ~~right~~ directly after exit) (Schumann, 1996). The slope of this mixing line is given by:

$$G = \frac{c_p EI_{H_2O} p_a}{0.662 Q(1-\eta)} \frac{c_p EI_{H_2O} p_a}{0.622 Q(1-\eta)}, \tag{1}$$

where c_p is the isobaric specific heat of air, EI_{H_2O} is the mass emission index of water vapour, p_a the ambient air pressure, η the overall propulsion efficiency, Q the specific heat of the fuel and 0.622 is the ratio between the molar masses of water and air. The ~~SAC is then the~~ ambient temperature at which the mixing line is tangential to the saturation curve with respect to water (saturation water vapour pressure curve) fulfils the SAC. Any lower ambient temperature will lead to the mixing line crossing the saturation curve and a period of supersaturation in the plume, while for higher ~~temperatures~~ ambient temperatures, no supersaturation with respect to water will be reached. In general, the steeper the slope G of the mixing line~~G~~, the higher the supersaturation in the plume for the same ambient conditions and the more water available to form droplets. The mass emission index of water vapour and the specific heat of the fuel have a large influence on G, as can be seen from Eq. (1). For ~~jet-A~~ Jet-A fuel we have $\mathrm{EI_{H_2O,J}} = 1.23$ kg (kg fuel)$^{-1}$ and $\mathrm{Q_J} = 43.2$ MJ (kg fuel)$^{-1}$ ~~in comparison~~ compared to $\mathrm{EI_{H_2O,H_2}} = 8.96$ kg (kg fuel)$^{-1}$ and $\mathrm{Q_{H_2}} = 123$ MJ (kg fuel)$^{-1}$ for hydrogen. ~~All else equal~~ Everything else being equal, this gives a slope for hydrogen that is approximately 2.6 times steeper than for standard Jet-A fuel. In addition ~~,~~ to larger supersaturations in the plume at the same ambient temperatures, the steeper slope for hydrogen as fuel ~~also~~ enables contrail formation at higher ambient temperatures, approximately 10K above conventional Jet-A fuel (Schumann, 1996).

The Schmidt-Applemann criterion predicts quite accurately when contrails can form, but for ~~the contrail to persist~~a formed contrail to become persistent, the ambient air needs to be supersaturated with respect to ice. If both these criteria are fulfilled, a contrail can form, persist ~~,~~ and potentially evolve into a contrail cirrus. Also, the properties of the ~~persistent contrail /~~contrail cirrus depend on the ~~amount~~ number and type of particles present for activation into water droplets. ~~With~~ If a larger number of particles is present, a larger number of droplets can form. The ~~amount~~ number of water droplets will also depend on the readiness of the present particles to act as condensation nuclei, that is, their hygroscopicity and size distribution. The hygroscopicity of substances can be roughly captured ~~with~~ using a single parameter κ ~~(Petters and Kreidenweis, 2007)~~ and for ambient particles~~it~~, this lies in the range $\kappa = 0.1$-0.9 (Petters and Kreidenweis, 2007). The higher the κ of a substance, the lower the supersaturation required for it to act as condensation nuclei for water droplets. ~~Same for size , the~~ The particle size can affect its ability to act as condensation nuclei for water droplets. The smaller the initial ~~aerosol~~ particles, the higher the supersaturation required for ~~it~~ them to act as condensation nuclei for water droplets. Supersaturation s is the water saturation ratio S minus one, $s = S - 1$. The κ-Köhler equation gives the water saturation ratio ~~S (where supersaturation s is saturation ratio minus one $s = S - 1$)~~ for the equilibrium wet diameter D for a particle/solution of dry diameter D_d:

$$S(D) = \frac{D^3 - D_d^3}{D^3 - D_d^3(1-\kappa)} \cdot e^{\left(\frac{4\sigma_{s/a} M_w}{RT\rho_w D}\right)}, \tag{2}$$

where $\sigma_{s/a}$ is the surface tension of solution/air interface, ρ_w the density of water, M_w the molecular weight of water, R the universal gas constant and T the temperature. The exponential part of ~~eq~~Eq. 2 instantiates the Kelvin effect, which describes how the saturation water vapour pressure increases over a curved surface. As can be seen~~the exponential~~, the exponential part approaches infinity as the wet diameter approaches zero (curvature increases)~~, this is because~~. This is because the more curved a surface is, the less energy is needed for a water molecule to evaporate ~~the more curved a surface is~~ and therefore the equilibrium saturation water vapour pressure is increased. The maximum ~~of~~ on the κ-Köhler curve gives the critical saturation ratio S_c, that is, the minimum saturation ratio needed for a particle with a certain dry diameter and κ to grow indefinitely ~~according to theory (although being limited~~ as theorised (and yet limited in reality by the atmospheric water budget~~in reality) orequivalently~~) or, as an equivalent, the minimum dry diameter needed at a certain saturation ratio. The minimum dry diameter/radius is referred to as the activation diameter/radius r_{act}~~and particles~~. Particles with $r > r_{\text{act}}$ in an environment with $S > S_c$ are said to be activated. Because of the Kelvin effect, the critical saturation ratio for small particles is increased~~, a small κ is also seen from~~. As seen in Eq. (2)~~to~~, a small κ does also increase the critical saturation ratio for a ~~certain~~ given dry radius.

3 Models and implementation

For our investigation into contrail formation and ~~the climate impact~~ energy forcing consequences of hydrogen aircraft, we ~~use~~ combine two models. ~~To approximate the amount~~ We use the theoretical model suggested by Kärcher et al. to approximate the number of ice particles formed in the exhaust under various conditions ~~we use the theoretical model put forward by Kärcher et. al (Kärcher et al., 2015)~~ (subsequently referred to as K15) but modify it to account for particles with ~~a very low hygroscopicity~~ low hygroscopicities (subsequently referred to as modified K15) using the κ-Köhler model ~~(Petters and Kreidenweis, 2007)~~ (Kärcher et al., 2015; Petters and Kreidenweis, 2007). The number of ice particles predicted ~~in this way is then~~ is subsequently used as input for CoCiP ~~(Contrail Cirrus Prediction model) constructed by Schumann (Schumann, 2012) for simulating~~ (Schumann, 2012), in its gridded formulation as implemented in the pycontrails repository (v0.54.1) (Engberg et al., 2025) (and henceforth referred to as simply CoCiP) to simulate contrail lifetime and its radiative impacts.

3.1 Theoretical model for ice particle formation, κ-köhler theory and activation emulators

3.1.1 Particle activation - model overview

The K15 model ~~has the capacity to predict microphysical and optical properties of contrail particles~~ is a tractable model that considers the microphysical pathway to contrail formation during the first few seconds after exhaust. ~~The model predicts, among~~ Among other things, the model calculates the number of ice particles that form from exhaust and entrained particles under given ambient conditions, engine ~~parameters and the particles'~~ characteristics, particle properties, emission numbers ~~or~~ and ambient concentrations. The relationshipbetween particle size, hygroscopicity, saturation ratio and activation in K15 is given by an approximation ~~to~~ derived from the κ-Köhler ~~theory~~ equation given in Eq. (2) ~~, and the saturation ratio in the plume over time is given by the ratio of the partial water pressure for the mixing line over the saturation water vapour pressure curve~~(Petters and Kreidenweis, 2007). The K15 model approximates the number of water droplets formed by equating ~~on the one hand the~~ the possible number of droplets that can form at a certain supersaturation along the mixing line (Eq. (37) in ~~K15) with on the other hand the~~ (Kärcher et al., 2015)) with the number of these particles needed to deplete the supersaturation at the point when the production rate of supersaturation equals the loss of supersaturation due to condensation (Eq. (51) in ~~K15). The~~ (Kärcher et al., 2015)). At the time when these two calculations of droplet particle numbers are equal, the particles are said to "quench" the supersaturation of the plume and no more particles can be activated into water droplets. The plume might still be supersaturated with respect to water after ~~quench~~ quenching, although not enough to activate the remaining unactivated particles. With the remaining supersaturation, the formed droplets can continue to grow by condensation until the supersaturation is ~~completely~~ depleted or the plume reaches the freezing temperature estimated by K15 (Eq. (36) in (Kärcher et al., 2015)), at which point droplets freeze into ice particles. Thus if freezing occurs, the number of ~~water droplets at quench equals the number of~~ ice particles formed is equal to the number of water droplets at quenching.

A crucial difference between the model and actual formation of water droplets from plume aerosols is that~~in reality~~ , in reality, droplets would form continuously and successively deplete the supersaturation~~leading~~ . This would lead to a decreasing ability to activate particles with low hygroscopicity and/or small ~~radius~~radii. The model may therefore overestimate the activation of small and/or low-hygroscopicity ~~exhaust particlesbecause of lower ability to activate and due to an underestimation of the~~ particles, since all particles activate instantaneously at quench. K15 may also overestimate the activation of low hygroscopicity and/or small particles due to the lack of competition for water between ~~ambient aerosols and exhaust particles , since lower supersaturation would promote~~ plume particles in the model. Lower levels of supersaturation would otherwise suppress the activation of ~~ambient aerosols with higher hygroscopicity over small and~~lower hygroscopicity and/or smaller particles in favour of large, high-hygroscopicity particles (Lewellen, 2020). Another limitation of the K15 model comes from the absence of the Kelvin effect in the formulation of the loss of supersaturation due to condensation (condensation sink L_w in (Kärcher et al., 2015)). This makes it possible for smaller numbers of activated particles to quench the plume, as outlined in (Ponsonby et al., 2025). This, in turn, leads to short quench-times and lower maximum supersaturations being reached in the plume, compared to more resolved models. This likely results in underestimations of the number of ice particles formed from small and/or low-hygroscopicity ~~exhaust particles (Lewellen, 2020).~~ particles. Hence, the K15 and modified K15 models have certain limitations of which the reader should be aware.

3.1.2 Homogeneous droplet nucleation and NO_x assisted nucleation

Homogeneous droplet nucleation (HDN) is a potential pathway to the formation of water droplets in the absence of aerosols (condensation nuclei). This pathway requires high levels of supersaturation to become active. The relatively high degree of water supersaturation in the exhaust of hydrogen-powered aircraft is expected to increase the likelihood of this formation pathway. This was investigated in (Zink et al., 2025a) and based on activation rate regions in T_a-p_a space where HDN could have an impact. The greatest impact occurred when ambient aerosol concentrations were low ($10^0 \mathrm{cm}^{-3}$) or zero. However, in such cases, it was reasoned that HDN probably would not generate greater overall numbers of ice crystals than ambient aerosols would (although this was not explicitly investigated). We have omitted HDN in our analysis, as its impact is likely minor for medium-to-high ambient aerosol concentrations.

NO_x emissions from hydrogen combustion may provide additional pathways affecting contrail particle formation. In particular, particle formation could be influenced either by the formation of nitrate-containing ion clusters or by modification of lubrication-oil-derived droplets through uptake of HNO_3 (nitric acid) (Fritz et al., 2020; Zink et al., 2025b). In soot-free conditions, the latter may be the more plausible pathway, since nitric acid is expected to be rapidly taken up by existing aerosol and contrail particles, whereas the former has not been shown to generate a substantial particle population on its own (Voigt et al., 2010; Wang et al., 2020) . Because these effects remain highly uncertain, we do not include them explicitly.

3.1.3 Activation of lubrication oil particles - approximations

The hygroscopicity of lubrication oil is ~~uncertain but~~ known to be low. ~~In (Ponsonby et al., 2024) it is shown~~ One study shows it to be consistent with $\kappa = 0$ for droplets of lognormal ~~distribution and mean radius 100 nm , in another study~~ size distribution and a geometric mean radius of 50 nm (Ponsonby et al., 2024). Another study estimated an upper limit for lubrication oil ~~is estimated to~~ as $\kappa = 6 \cdot 10^{-4}$ (Lambe et al., 2011). We have ~~implemented a modification to~~ modified the approximate expression ~~for~~ of the critical supersaturation (maximum of Eq. (2)) and activation radius ~~from (Petters and Kreidenweis, 2007)~~ used in K15, to account for the low hygroscopicity of lubrication oil. The ~~original approximate expression in (Petters and Kreidenweis, 2007) is~~approximate expression is:

$$s \approx \ln(S) = \sqrt{\frac{(r_k/r_{act})^3}{54\kappa}}, \qquad (3)$$

where s is the supersaturation, S the water saturation ratio ~~,~~ and r_k is the Kelvin radius. The Kelvin radius is set to 1 nm in K15 but equal to $r_k = \frac{4\sigma_{s/a} M_w}{RT\rho_w}$ in Petters ~~, M. & Kreidenweis , S.~~ and Kreidenweis and in our study. This approximation of the correlation between the critical supersaturation and activation radius is good for $\kappa > 0.2$ ~~(Petters and Kreidenweis, 2007) but becomes increasingly worse~~ and large, dry radii but deteriorates for substances with smaller κ and dry radii of approximately < 10nm (Petters and Kreidenweis, 2007; Ponsonby et al., 2025). Our correction to Eq. (3) ~~is non-physical in the sense that it is not derived from first principles but rather~~ relies on a parametrisation based on a ~~minimization~~ minimisation of the error between ~~the approximation of~~ Eq. (3) and the critical saturation ratio maximum from Eq. (2) for small κ-values ~~, more~~ and all dry radii. More details can be found in Supplement~~ary~~ S2. The ~~corrected~~ updated equation for the activation radius is:

$$r_{act} = \alpha_0 \kappa^{\alpha_1} s^{-2/3} \frac{r_k}{(54\kappa)^{1/3}} \tag{4}$$

where ~~$\alpha_0 = 1.16788$ and $\alpha_1 = 0.186086$~~ $\alpha_0 \approx 1.2$ and $\alpha_1 \approx 0.19$. We have calibrated the ~~correction~~ update such that $\alpha_0 \kappa^{\alpha_1} \approx 1$ for $\kappa = 0.5$. For $\kappa > 0.5$ ~~no correction~~ , no change is needed since Eq. (3) is valid. We refer to the K15 model with this update as the "modified K15 model".

The K15 model can incorporate any number of particle types with lognormal size distributions and varying hygroscopicities from either exhaust or the ambient atmosphere. If multiple particle types are present in the plume ~~the model utilises~~ , the quench time is calculated using weighted averages of the ~~particle types activation radii~~ activation radii, r_{act} ~~(~~ and slope parameters ~~, see supplementary~~ of the respective particle types (see Supplement S3) ~~for obtaining the quench time, calculated as droplet number weighted~~ . The effective averages are calculated as droplet-number-weighted averages of the different activated particle types. Thus, the model uses averages to obtain the ~~time of quench~~ quench time but also keeps track of the number of each particle type that ~~is~~ are activated into water droplets ~~calculated with~~ . The latter is calculated using an estimated activation fraction for each particle type (ϕ_l in K15 Eq. (37) and (40)) multiplied by the respective number of particles or concentration of each type ~~respectively~~ in the plume. ~~Our model implementation needs~~ For implementation in CoCiP, our new ice particle number module requires the number of ~~activated droplets from~~ droplets activated by each particle type at the ~~time of quench for implementation in CoCiP. Thus~~ moment of quenching. Thus, we created emulators (or fitted functions) ~~to the activation fraction at quench to~~ for the activation fractions at quench that we use in CoCiP. This is done ~~for shortening runtimes~~ in our updated version of CoCiP, since the K15 model does not supply a closed expression for the number of ice particles formed but estimates it ~~from~~ based on the equality of the two expressions of activated droplets mentioned above (Eq. (37) and (51) in K15). The solution to the equality ~~can be found by~~ may be found using numerical methods. ~~Implementation of this for every waypoint~~ Finding the solution to this equality for every gridpoint and flight level in CoCiP would be too ~~time intensive to cover all cases we wish to investigate~~ time-consuming for a global level analysis.

3.1.4 ~~Variation in size distributions~~ Emulators for lubrication oil and ~~properties~~ aerosol activation

The uncertainty and variability in the lubrication oil particle size ~~distribution is large because of the differences in oil handling by different engines ,~~ distributions are large because different engines release lubrication oil differently. It may be either vented or leaked, ~~in or beside~~ within or alongside the exhaust. ~~For volatile lubrication oil~~ Lubrication oil ending up in the exhaust ~~this implies it~~ is heated and vaporised and needs time to form droplets ~~which in turn effects the characteristics of the~~ . The temperature and time affects the particle size distribution ~~. Larger oil droplets from oil-venting is mostly captured for re-use which in a study gave~~ characteristics. Most larger oil droplets emitted through oil venting are captured for reuse. Based on experiments on aircraft engines at idle, the remaining vented droplets were estimated to have a volumetric mean ~~radii of 125-175 nm from an experiment of aircraft engines in idle~~ radius of 125–175 nm (Yu et al., 2010). A measuring campaign around Narita ~~airport~~ Airport in Japan reported smaller size distributions of radii < 15 nm (Fushimi et al., 2019).

Experiments using lubrication oil heated to two different temperatures and measured at room temperature show mean diameters of approximately ~10 nm and 27 nm for temperatures at of 300°C and 20°C respectively (Ungeheuer et al., 2022).

To handle the variability in size distribution our emulator for The probability function of a lognormal size distribution is given by $n(r) = \frac{N}{\sqrt{2\pi}}\frac{1}{\ln\sigma_o}\frac{1}{r}\exp\left[-\frac{1}{2}\left(\frac{\ln(r/\mu_o)}{\ln\sigma_o}\right)^2\right]$, with total number N, geometric mean radius μ_o and geometric width σ_o. To account for variability in the size distribution, the lubrication oil activation includes mean emulator includes μ_o and variance σ_o^2 of the lognormal size distributions, as well as variablesrelated to σ_o as input variables. It also includes variables describing the ambient conditions, which include namely ambient temperature T_a, relative humidity rh, air atmospheric pressure p_a and the critical saturation temperature T_c (from SAC). Hygroscopicityin terms of derived from the SAC. Hygroscopicity, measured by κvalue , was not included as a variable in the emulator, to limit the functional complexity, but . However, the functional form of the emulator can be made to fit different κ , more details of method to find functional form, parameters and span of validity values. More details of our method can be found in supplementary Supplement S3.1.

There is also a large variability in ambient aerosols (Raes et al., 2000; ?; ?; ?; ?). The largest source of upper tropospheric aerosols come from anthropogenic and natural emissions of precursors carried to high altitudes by updrafts (Minikin et al., 2003) which later form particles, but also from for example aircraft emissions (Righi et al., 2013). An estimated 30-40% of aerosols at northern mid latitudes at 7-12 km altitudes originate from aircraft (Righi et al., 2013). In measurement campaigns concentrations of ultrafine (radii > Likewise, ambient aerosols show considerable variability in size, concentration and hygroscopicity. Reported particle radii range from 5 nm) was found to be 180-830 cm^{-3} for the southern hemisphere and 450-15000 cm^{-3} in the northern in the upper troposphere and aitken mode aerosols (radii > 14 nm) 130-400 cm^{-3} for the southern hemisphereand 290-9600 cm^{-3} in the northern respectively. Accumulation mode (0.5-2 to 2 μm) was lower at 6-34 m and number concentrations range from 6 to 15,000 cm^{-3} for the southern and 16-90 cm^{-3} in the northern hemispheres (Minikin et al., 2003). Other campaigns also showed a large variability in concentration in the subtropics, tropical tropopause and mid-latitudes between 50 and over 1000 cm^{-3}in 9-12 km altitudes (Borrmann et al., 2010). Other studies have focused on estimating the hygroscopicity of aerosols and cloud condensation nuclei. One study over the north China plain found average values in the range of , depending on particle size and hemisphere. Concentrations are typically higher for smaller particles and are generally greater in the Northern Hemisphere (Raes et al., 2000; Clarke and Kapustin, 2002; Minikin et al., 2003; Borrmann et al., 201 . Reported hygroscopicity values range from 0.1 -0.4 (Liu et al., 2014), the κ-parameter to 0.4 (Liu et al., 2014; Padró et al., 2010) . To keep the emulator dimension manageable and given that the role of water-soluble compounds has been found to be around 0.28 ± 0.06 according to (Padró et al., 2010).

3.1.5 The emulators for lubrication oil and aerosol activation

Capturing all this variation explicitly would lead to a very large number of particle types to include in the K15 model. Since the effect of ambient aerosols in hydrogen contrail formation has been studied ice crystal formation in hydrogen contrails has previously been examined to some extent previously (Bier et al., 2024)we have instead put our focus on the variability of lubrication oil . We thus handle the large variability of ambient aerosols, as done in (Bier et al., 2024), we focus on uncertainties and variability in lubrication oil properties and emissions. Therefore, following previous studies (Kärcher et al., 2015; Bier et al., 2024), by lumping all together as one the substantial variability in ambient aerosols is represented by a single particle type with a representative size distributionand concentration . Ambient aerosols in addition to being activated also need time to get entrained into the plume. Our emulator of activated ambient aerosols at quench includes both entrainment and activation and gives the fraction of entrained activated ambient aerosols at quench given ambient conditions, represented by ambient temperature T_a, relative humidity rh, air pressure p_a and critical saturation temperature T_c (from SAC), more details can be found in supplementary S3.2. , concentration and hygroscopicity. A more comprehensive treatment is left to future work.

The respective activation functions for lubrication oils and ambient aerosols , respectively, emulate the output emulate the fraction of activated lubrication oil droplets and the level of entrainment and activation of ambient aerosols at quench obtained by the modified K15 model when both lubrication oil and ambient aerosols are included. Examples of output from In the model, mixing between exhaust and ambient air is not instantaneous. As a result, the concentration of ambient aerosols within the plume does not immediately reach the ambient background value and may still be lower than that of the surrounding air at the time of quench. The emulator for activated ambient aerosols at quench therefore accounts for both the difference between plume and ambient aerosol concentrations and for the fraction of the plume ambient aerosol concentration that becomes activated. Fig. 1 shows examples of outputs from the modified K15 and our emulators for both our emulators. This covers different lognormal size distributions of lubrication oil and ambient aerosols at at an atmospheric relative humidity of 60% relative humidity , % and for varying ambient temperaturesare shown in Fig. 1. As seen in Fig. 1 the fit . For lubrication oil (presented in the two left-hand columns), the largest deviations between the emulator and the output from the modified K15 is very good. The hardest casesfor the emulators to capture are when the activation of lubrication oil is low which occurs for small mean radius model are found for a geometric mean radius of 5 nm, combined with the smallest and largest geometric widths (1.28 and low hygroscopicity. Still, even in these cases the fit is decent, especially given the large uncertainties involved2.72) respectively. The two right-hand columns show ambient aerosol entrainment and activation. Across all ambient aerosol cases, lower values are obtained at lower temperatures because supersaturation increases more rapidly in the plume, which shortens the quench time. The shorter quench time reduces the time available for entrainment of ambient aerosols, thus yielding lower ambient aerosol concentrations in the plume at quench than in the surrounding air. More details can be found in Supplement S3.2.

In Supplement S6, we show the deviation of output from CoCiP when using the emulator to compare results as opposed to using the modified K15 model implemented directly in CoCiP. Using the emulator resulted in differences in mean energy forcing per flight meter of < 11% for all lubrication oil size distributions tested (except one outlier), with generally smaller deviations for larger radii. The outlier corresponded to a geometric mean radius of 3 nm and a geometric width of 1.28, and yielded a mean energy forcing per flight meter 22% lower than that obtained using the modified K15 model directly.

3.1.5 Base case implementation parameter values

The emulators are based on the modified K15 modeland κ-Köhler theory and in our base case settings implemented with . In our base-case setting, lubrication oil characteristics based on are represented by a lognormal size distributionwith , with geometric mean $\mu_o = 7.5$ nm and geometric width $\sigma_o = e^{0.375} \approx 1.45$consistent with oil size distributions found in (Ungeheuer et al., 2022), where . This is consistent with reported measurements, in which the oil was heated to 573 K and

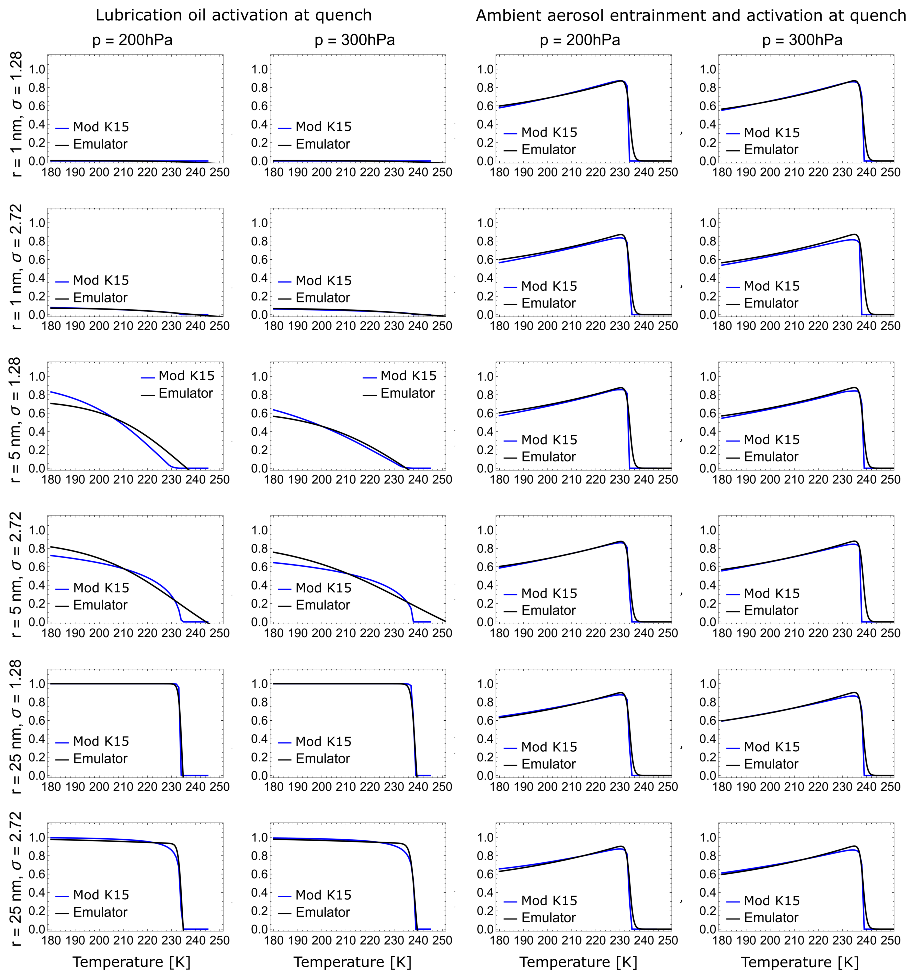

Figure 1. The figure shows ~~examples from~~ the share of particles activated into ice crystals using our emulators~~of~~, as compared to the modified K15 model. This is done for both lubrication oil ~~activation to~~ (the ~~left~~ two left-hand columns) and ambient ~~aerosol entrainment + activation to~~ aerosols (the ~~right together~~ two right-hand columns). All results were obtained with ~~activation output from the K15 model for an~~ atmospheric relative humidity ~~at~~ of 60% and for different assumptions on lubrication oil size distributions (rows) and atmospheric pressure (columns). ~~The~~ For lubrication oil, the lower activation due to the Kelvin effect for small particles (geometric mean radius ~~$r = 5$~~ $r = 1$ nm and $r = 5$ nm) is clearly seen ~~for lubrication oil~~ in the top ~~two~~ four rows.~~The lower entrainment + activation values for ambient aerosols at low temperatures is due to lower entrainment because of shorter times before quench at low temperatures.~~

~~then let~~ subsequently allowed to nucleate into droplets ~~. This size-distribution~~ (Ungeheuer et al., 2022). This size distribution for our base case is therefore on a par with the oil being ejected into the main exhaust (we assume $T_0 = 660$K). In ~~our base case~~the base case, the lubrication oil hygroscopicity is set to $\kappa_o = 6 \cdot 10^{-4}$, which is found as a maximum for lubrication oil ~~in~~ (Lambe et al., 2011). The base case lubrication oil droplet mass emission index ~~we~~ is set to $\mathrm{EI}_o = 2$ mg (kg fuel)$^{-1}$, based on two studies . The first of these studies on kerosene enginesshows an increase in of kerosene engines. The first study indicates a power-related increase in the oil emission index with power and an emission index range of 2-12 mg (kg fuel)$^{-1}$ (Yu et al., 2010). The other second study found rather little dependence on powerand emission indices . The emission indices were in the range of 1-2 0.5-2 mg (kg fuel)$^{-1}$with an , with one outlier engine at 40 mg (kg fuel)$^{-1}$ (Timko et al., 2014) and highly dependent on the type of engine and the type of lubrication oil lubrication oil (Timko et al., 2014). Both studies have measured droplets of lubrication oil, thus only allowing the lubrication oil which has managed to form droplets to be measuredwithout accounting for the possibility that a fraction of the emitted oil could have remained in the vapour phase. A third study instead estimated the oil emission index from the amount based on the amount of oil used by the engine and obtained a much higher estimate of 110 mg (kg fuel)$^{-1}$ (Decker et al., 2024). Our lubrication oil emission indices are based on measured droplet emission indices and we therefore assume that all the oil mass in our study is in the form of droplets which can act as condensation nuclei. Since no values for hydrogen combustion were found in the literature, we use measured kerosene combustion values as bases for our oil emission index for hydrogen combustion. We use kerosene values even though differences in, say, specific heat might actually give different values per meter. To test the model sensitivity to this assumption, we conducted a sensitivity analysis. In this analysis, we use the value $\mathrm{EI}_o = 20$ mg (kg fuel)$^{-1}$ which is large, but not larger than the outlier in one of the studies mentioned (Timko et al., 2014).

For the lognormal size distribution for the ambient aerosol of the ambient aerosols, we set the geometric mean radius to $\mu_a = 15$ nm and standard deviation geometric width to $\sigma_a = 2.2$in line with (Kärcher et al., 2015) , to cover a broad range of particle sizes. The hygroscopicity value is set to $\kappa_a = 0.5$ and the ambient concentration to $n_a = 1000$ cm^{-3}both values quite high ($n_a = 600$ cm^{-3} used in (Bier et al., 2024) for example)in order to not underestimate the impact of ambient aerosols' contribution to ice particle formation, in line with the literature for similar models (Kärcher et al. (2015), Bier et al. (2024), Yu et al. (2024)).

It should be noted that we are using the emulator of the modified K15 model under the conditions (small particle sizes and low hygroscopicity for lubrication oil) where the K15 model and hence our emulators, most certainly overestimates the amount which allow the model (and consequently our emulator) to underestimate the number of activated particles due to the condensation sink formulated without the Kelvin effect. Hence, the number of ice particles formed from lubrication oil will likely be slightly overestimatedunderestimated, especially for size distributions with small mean radius and for small values for the standard deviationgeometric mean radii and small geometric width values (Ponsonby et al., 2025).

In cases when we simulate contrail formation for fossil jet fuel, we do not use an emulator of the modified K15 for the activation, but we use the standard approach in CoCiP. However, if the for fossil jet fuel combustion, using an emulator of the modified K15 model had been used to find the activation of to represent soot and ambient aerosols for fossil jet fuel combustion we get activation almost identical to the activation functionused in CoCiP for soot , see supplementary aerosol activation would have yielded almost identical particle activation to that predicted by CoCiP's existing soot activation function. A comparison of the modified K15 model implemented directly in CoCiP with CoCiP's native soot activation function is shown in Supplement S6.

3.2 Contrail Cirrus Prediction model

~~CoCiP is a Lagrangian plume model that simulates contrail cirrus formation, development and climate impact in terms of energy forcing and radiative forcing (Schumann, 2012). It can be run either along flight paths or in a gridded modewith~~ For CoCiP in the gridded mode, the model output is based on a test flight ~~flying~~ of 1 km in the middle of the grid cells. For the simulation and ~~calculations of contrail cirrus~~ contrail cirrus calculations, CoCiP incorporates meteorological data and flight performance parameters. ~~Any aircraft performance calculator can be used such as Eurocontrols BADA family (Nuic et al., 2010) but CoCiP also has a built in aircraft performance model, the Poll-Schumann model (Poll and Schumann, 2021a, b, 2025) to obtain the performance variables such as fuel flow and engine efficiency, and non-volatile particulate matter (nvPM) emission number.~~

CoCiP u~~tili~~ses a monodisperse particle size distribution ~~of~~ for ice particles once formed. The number of ice particles obtained ~~from activation share the ice~~ in the activation calculation stage share the water content of the plume equally~~and~~. The properties of the plume, ~~for example~~ such as the sedimentation rate, are calculated using an effective mean ice particle volumetric radius (Schumann, 2012). ~~Radiative forcing however is calculated using~~ The optical depth and radiative forcing are calculated using an assumption of different habits (shapes) of ice particles~~. CoCiP uses distributions of ice particle habits with up to three different habits out of eight possible, depending~~ , in which the mixture depends on the effective volumetric radius and ~~based on when different habits are assumed to be prevalent. The habits have their own calculated effective radius and thus reflective area, such that the habit distribution influences the optical depth and the radiative forcing of the contrail cirrus~~ evolution of the plume (Schumann et al., 2011, 2012).

~~In this study we use the gridded version of CoCiP from the open-source pycontrails repository (v0.54.1). When running~~ When running CoCiP in gridded mode, a model aircraft is chosen ~~. We chose to~~ for which we use the aircraft with ICAO aircraft designator B737. ~~It is~~ This is the default in CoCiP grid and is one of the most common aircraft families (B73X)~~and also default in CoCiP grid~~. We use ~~CoCiPs built in~~ the aircraft performance model available in pycontrails, the Poll-Schumann model. This ~~means we obtain soot emission numbers for jet propulsion in the order of $\sim 10^{15}$ in the high soot regime. One could argue a comparison to lower soot emission numbers would be preferable mimicking a future kerosene fleet (in the same time-frame as a possible hydrogen fleet). In the lower soot regime however, there are still large uncertainties regarding the ability of ultrafine emission particles to form ice particles, significantly so at low temperatures, resulting in an increase in climate impact from contrail cirrus (Kärcher and Yu, 2009; Yu et al., 2024). Therefore we chose to make our comparison with the well known effects of jet aircraft in the high soot regime.~~ model will generate soot emissions for jet fuel propulsion, on the order of $10^{15}(\text{kg fuel})^{-1}$.

~~In this first implementation of hydrogen in CoCiP we use the built in CoCiP hydrogen fuel and our emulators for lubrication oil and ambient aerosol ice particle activation although we do not model a hydrogen aircraft, meaning we use the same B737 aircraft performance output such as true airspeed, aircraft weight for kerosene as well as for hydrogen fuel. This is a simplification for an actual hydrogen aircraft. Hydrogen has a higher energy content per unit mass than kerosene but a lower energy per unit volume and is in gas phase at atmospheric flight level conditions. Most hydrogen aircraft conceptual models and prototypes utilise compressed and cold liquid hydrogen which leads to fuel systems with higher complexity and tank volumes~~

~~still larger than for kerosene. A measure of fuel system efficiency often used is Gravimetric Index (GI = fuel weight at full tank / (fuel weight at full tank + fuel system weight) reported in percent), measuring the share of fuel weight to the entire fuel system. Fuel system usually refers to all structures needed to store fuel such as tanks and piping. For jet fuel, the gravimetric index is close to 100% because the tanks are integrated into the wings. A bit simplified, lower gravimetric index adds to weight and drag of the aircraft increasing both power and energy needed for same flight patterns as jet flights.~~

~~To simulate the implications of different GI we utilise two modifications for hydrogen fuel on energy expenditure and fuel flow. Either we use energy expenditure corresponding to 1.6 times the energy expenditure for kerosene (Energy Consumption Ratio, ECR= 1.6) giving an upper estimation consistent with GI= 20% and energy usage in (Adler and Martins, 2023) (same GI gives approximately ECR= 1.2 for mid-range aircraft in (Mukhopadhaya and Rutherford, 2022)). This corresponds to a modification of fuel flow for hydrogen according to~~ $\mathrm{ff}_{\mathrm{H_2}} \approx 0.56\, \mathrm{ff}_{\mathrm{J}}$ ~~because of the higher energy content per mass. In a more optimistic modification we set the energy consumption ratio to one (ECR= 1) consistent with a gravimetric index of GI= 55% and the break even point in (Adler and Martins, 2023) (and CoCiP default for hydrogen fuel). We anticipate that an actual hydrogen aircraft will fall somewhere in between these fuel flow boundaries and leave an accurate modelling of the energy use of a hydrogen fleet to future studies.~~

~~As meteorological input~~For meteorological input, we use the high resolution (HRES) ERA5 reanalysis data provided by the European Center for Medium-range Weather Forecasts (ECMWF) ~~(Hersbach et al., 2020) for the year 2019.~~ for 2019 (Hersbach et al., 2020). The HRES ERA5 data has a latitude/longitude resolution of $0.25° \times 0.25°$ and pressure levels between 1-1000 hPa. We have used either a range of flight levels of 100-600 hPa or the most common flight levels 200-300 hPa for different investigations. ~~One of the important variables in the ERA5 dataset is relative humidity with respect to ice (RHi), which determines if a contrail will persist or not.~~ Studies have highlighted the fact that ERA5 RHi ~~are usually weakly supersaturated and tend~~ tends to underestimate high supersaturations compared to actual measurements (Gierens et al., 2020; Rädel and Shine, 2010; Reutter et al., 2020). When running CoCiP we therefore use ~~the humidity scaling proposed by (Teoh et al., 2022a)~~ one of the humidity scalings included in the pycontrails package (Teoh et al., 2022a).

When we run CoCiP with ~~hydrogen as fuel we utilise~~ an aircraft powered by hydrogen combustion, we use our emulators for lubrication oil activation A_o and ambient aerosol ~~activation A_a~~entrainment plus activation EA_a. We obtain the ice particle number per meter after downwash N_{ice} for ~~both~~ lubrication oil and ambient aerosols according to:

$$N_{\text{ice}} = \left(A_o \frac{ff}{v_{\text{tas}}} EI_{\text{n,o}} + E A_a n_a A_{\text{plume}} n_{\text{engine}} \right) f_{\text{surv}}, \tag{5}$$

where ff (kg s^{-1}) is the fuel flow, v_{tas} (m s^{-1}) the true airspeed, $EI_{\text{n,o}}$ ((kg fuel)$^{-1}$) the lubrication oil droplet number emission index, n_a (m^{-3}) the ambient aerosol concentration, A_{plume} (m^2) the cross-sectional area of the plume at quench, n_{engine} the number of engines of the aircraft and f_{surv} ~~CoCiPs~~ CoCiP's survival fraction after the vortex downwash. More details can be found in ~~supplementary~~ Supplement S4. ~~This is the ice particle number per meter after the downwash~~

3.2.1 Hydrogen aircraft model

Table 1. Parameter settings for our base case of hydrogen combustion.

Parameter	Notation	Value	Unit
Ambient aerosol geometric mean radius	μ_a	15	nm
Ambient aerosol standard deviation geometric width	σ_a	2.20	nm -
Ambient aerosol hygroscopicity parameter	κ_a	0.5	-
Ambient aerosol concentration	n_a	1000	cm^{-3}
Lubrication oil geometric mean radius	μ_o	7.5	nm
Lubrication oil standard deviation geometric width	σ_o	$e^{0.375} \approx 1.45$	nm -
Lubrication oil hygroscopicity parameter	κ_o	$6 \cdot 10^{-4}$	-
Lubrication oil droplet emission index	EI_o	2	mg (kg fuel)$^{-1}$
Engine exhaust temperature	T_0	660	K
Gravimetric index GI 55 %Energy consumption Energy usage ratio ($E_{\mathrm{H_2}}/E_{\mathrm{J}}$)	ECR EUR	1	-

We do not model a hydrogen aircraft explicitly. Rather, we use the same B737 aircraft performance output such as true airspeed and aircraft weight as for fossil jet fuel but make adjustments to the energy usage for the same aircraft performance. Most conceptual models and prototypes of hydrogen aircraft use cryo-compressed liquid hydrogen which leads to fuel systems of higher complexity and larger tank volumes than for fossil jet fuel. This generally leads to a lower fuel weight to fuel-plus-fuel-system weight ratio and increased drag compared to fossil jet fuel aircraft. This, in turn, may increase both the power and energy needed for the same flight patterns as fossil jet fuel flights, despite the higher energy content per unit mass of hydrogen.

The more important We consider two alternative assumptions for the energy use of hydrogen aircraft. One is relatively pessimistic and assumes an energy usage ratio of EUR$=1.6$, meaning that a hydrogen aircraft requires 1.6 times as much energy as a fossil-jet-fuel aircraft. This is consistent with hydrogen aircraft fuel-system assumptions in the literature (Adler and Martins, 202 , although reported EUR values vary even under similar technical assumptions; for example, (Mukhopadhaya and Rutherford, 2022) assumed approximately EUR$=1.2$ for a mid-range hydrogen aircraft. The other, which we adopt as our base case, assumes an energy usage ratio of EUR$=1$, corresponding to the default energy use for hydrogen fuel in CoCiP. We anticipate that an actual hydrogen aircraft will fall somewhere between these energy usage boundaries. We leave an accurate modelling of the energy use of a hydrogen fleet to future studies.

Key parameter choices for our base case are listed in Table 1more detailed parameter setting . Equivalent parameters for fossil jet fuel, such as nvPM emission index, are generated in the aircraft performance module in CoCiP. More detailed parameter settings for the models can be found in supplementary Supplement Table S1.

4 Results

4.1 Comparing contrail cirrus climate effect from jet and hydrogen combustion aircraft.

To compare the contrail cirrus climate effects generated by fossil jet fuel and hydrogen combustion aircraft, we simulate contrail cirrus formation and properties for ~~the whole year~~ all of 2019 on a global grid~~with 1~~, with one degree latitude and longitude resolution for both types of fuel. ~~Our base parameter settings for hydrogen for ice particle formation are shown in Table 1. Equivalent parameters for fossil jet fuel, such as nvPM emission index, are generated in the aircraft performance module in CoCiP.~~ In Fig. 2 ~~we show in panel~~ panels (a) and (b) ~~the global 2019 probability~~ show the estimated relative frequency of persistent contrail cirrus ~~,~~ formation; in (c) and (d), the estimated average contrail lifetime~~, and~~ ; and in (e) and (f)~~average Energy Forcing~~ , the estimated average EF per contrail generating flight meter (EFpcm), for both ~~fuels (Hydrogen left column,~~ hydrogen (left-hand column), plus fossil jet fuel ~~right~~ (right-hand column) averaged over longitude ~~, for latitude vs. altitude.~~ and time, for different latitudes and altitudes. As can be seen, the ~~general patterns are similar between the two fuels~~ two fuels have some general patterns in common, although there are ~~some~~ notable differences. As expected from the SAC~~the probability~~ , the relative frequency of contrail cirrus formation is higher at lower altitudes for hydrogen than for fossil jet fuel due to the ~~larger~~ greater emission intensity of water vapour for hydrogen. Further, a shorter average ~~contrail lifetime of hydrogen contrail cirrus~~ lifetime for contrail cirrus formed by hydrogen aircraft is clearly seen when comparing panels (c) and (d) of Fig. 2. ~~The shorter lifetime is because a~~ On average, the lifetime is 39% shorter for contrail cirrus formed from hydrogen aircraft compared to those formed from fossil jet fuel aircraft. This shorter lifetime is a consequence of the fact that a smaller number of ice particles are activated for hydrogen combustion than for fossil jet fuel combustion. This implies that ~~more ice will deposit on~~ each ice particle ~~(~~contains a larger share of the available ice water content, since in CoCiP the ~~available~~ ice water content is ~~shared equally by all particles), which in turnimplies that the mass of the particle will grow fasterand also will sediment faster causing a reduction in~~ distributed equally among all particles. This, in turn, will imply that the sedimentation is faster, resulting in shorter average contrail lifetimes (Lewellen et al., 2014; Kärcher, 2016). The ~~lower lifetimes in turn~~ shorter lifetime contributes to the ~~lower EFpcm seen for hydrogen compared to jet in the~~ EFpcm being lower for contrail cirrus formed by hydrogen aircraft compared to fossil jet fuel aircraft, as shown in panels (e) and (f)~~panels~~ , respectively (note the difference in scale).

~~Comparison of 2019 longitudinal averages between jet and hydrogen persistent contrail cirrus. Top panels (a) and (b) show the probability of persistent contrails. The middle panels (c) and (d) show the average contrail lifetime and the bottom panels (e) and (f) show average energy forcing per contrail forming flight meter (EFpcm). Note the difference in scale for the EFpcm between hydrogen and jet plots. Hydrogen simulations are run with with base setting $GI = 55$, $\kappa = 6 \cdot 10^{-6}$, $EI_o = 2$ mg (kg fuel)$^{-1}$ and lognormal size distribution LogNormal($\mu_o = 7.5$ nm, $\sigma_o \approx 1.45$) for lubrication oil and, $\kappa = 0.5$ and LogNormal($\mu_a = 15$ nm,$\sigma_a = 2.2$) for ambient aerosols.~~

~~Although~~ However, although lower average contrail lifetime does contribute to a lower ~~EFpcm the largest decrease~~ average EFpcm, the largest impact comes from the reduction in the reflective area of ~~all ice particlesfollowing the lower~~ ice particles, as the number of ice particles for hydrogen combustion compared to fossil jet fuel combustion is lower. The ice particles still share the same ice water content (as discussed above) but the area to volume ratio drops with a smaller number of particles. ~~The reduced~~ With a smaller ice particle area~~reduces~~ , the optical depth (and thereby radiative forcing and energy forcing~~(Lewellen et al., 2014; Kärcher, 2016).~~) drops (Lewellen et al., 2014; Kärcher, 2016). On average, the model output for EFpcm is about 80% lower for hydrogen aircraft than fossil jet fuel aircraft due to the two mechanisms explained above.

In Fig. 3~~we see~~ , we show the average ice particle numbers after downwash for hydrogen and ~~jet after downwash for altitude vs. latitude~~fossil jet fuel aircraft per meter contrail formed and for different altitudes and latitudes. The ice particle number for fossil jet fuel aircraft is more than five times greater than for hydrogen aircraft over the whole span of latitudes and altitudes for which fossil jet fuel SAC is fulfilled. For hydrogen aircraft, the ice particle contributions from ~~lubrication oil and ambient aerosols~~ ambient aerosols and lubrication oil are shown separately in panels (~~b~~a) and (~~a~~b) respectively in Fig. 3. Ice particle numbers from lubrication oil ~~is~~ are seen to be lowest at lower altitudes because of higher temperatures generally leading to lower supersaturations in the plume ~~in general and~~ and therefore lower activation of the lubrication oil droplets. ~~On the contrary~~ Indeed, ice particle numbers from ambient aerosols show an increase at lower altitudes. This is because the limiting factor for ice particle formation from ambient aerosols is ~~rather~~ the time window for particles to get entrained into the plume ~~. With lower activation of lubrication oil~~ before quench, rather than the magnitude of the supersaturation in the plume. With a lower number of activated particles from lubrication oil and thus a smaller condensation sink, it takes longer to quench the supersaturation of the plume~~and hence~~ . Consequently, more ambient aerosols ~~can be entrainedand~~ get entrained, become activated and form ice particles at higher temperatures ~~/lower altitudes. This~~ (and lower altitudes). This entrainment and activation behaviour can be seen in Fig. 1~~where the~~ , in which the entrainment and activation for ambient aerosols is seen to drop at lower temperatures. ~~The ice particle number for jet is more than 5 times larger than for hydrogen over the whole span of latitudes and altitudes where fossil jet fuel SAC is fulfilled.~~

To better see the total potential impacts of hydrogen and fossil jet fuel aircraft, we combine the effect of contrail cirrus formation ~~probability and EFpcm , and~~ frequency and EFpcm to estimate the average ~~Energy Forcing~~ energy forcing per flight meter (EFpfm). The result is shown in Fig. 4 for ~~both hydrogen~~ hydrogen aircraft (a) and ~~jet~~ fossil jet fuel aircraft (b)~~aircraft and we see that even if the probability of formation is larger for hydrogen , this~~ . The global average EFpfm (averaged over altitude, longitude, latitude and time) is reduced by 66% for hydrogen aircraft in our base case, compared to fossil jet fuel aircraft (note the difference in scale in Fig. 4). This, despite the higher relative frequencies of persistent contrail cirrus for hydrogen fuel. The higher relative frequencies for hydrogen aircraft only has a noticeable impact on EFpfm at relatively low altitudes. ~~However~~But even in this case, it is a modest effect ~~,~~ and hard to discern in Fig. 4. ~~The patterns again look similar for the two fuels, but the colour intensity used in the figure is different and the scale for fossil jet fuel is higher than that of hydrogen.~~

4.2 ~~Impact of lubrication~~ Lubrication oil ~~size distributions~~sensitivity analysis

4.2.1 ~~Lubrication oil sensitivity analysis~~

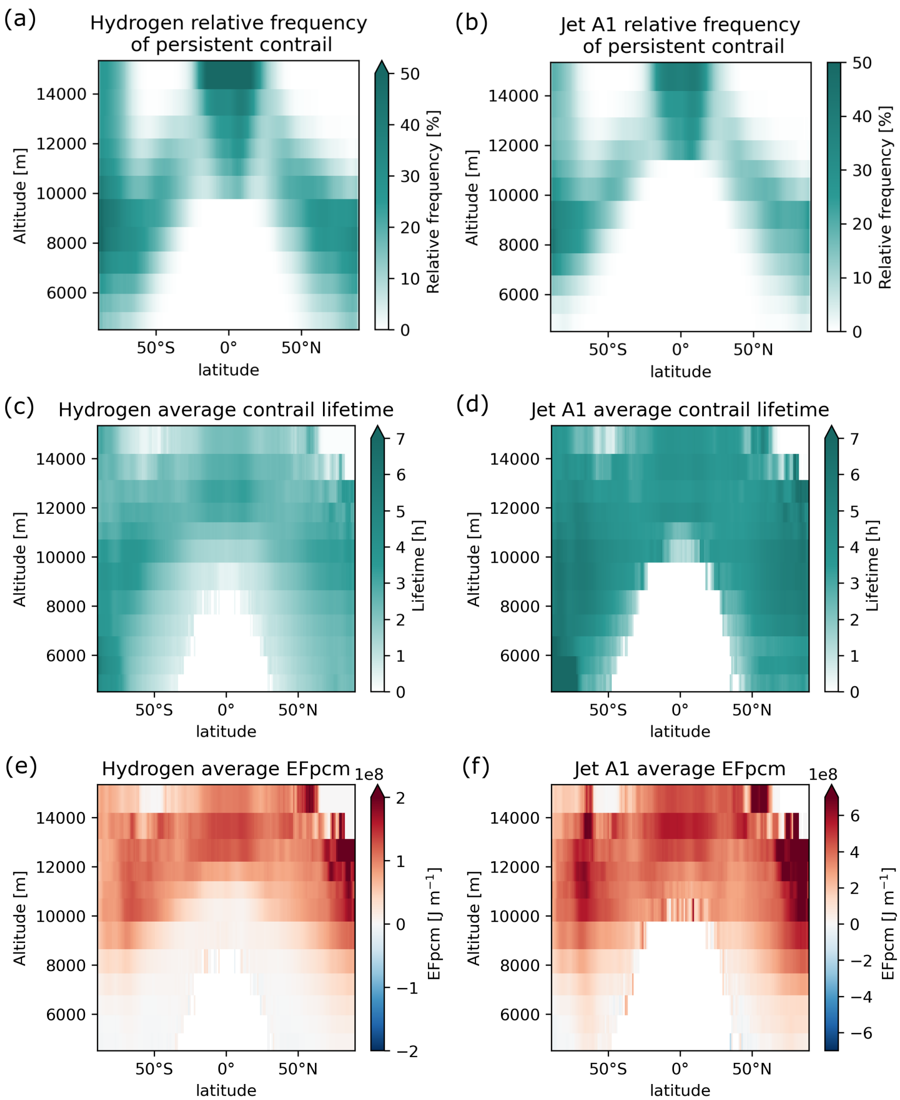

Figure 2. Comparison of 2019 longitudinal averages between jet and hydrogen persistent contrail cirrus. The top panels (a) and (b) show the relative frequency of persistent contrail formation. The middle panels (c) and (d) show the average contrail lifetime and the bottom ones (e) and (f) show average energy forcing per contrail forming flight meter (EFpcm). Note the difference in scale for the EFpcm between hydrogen and jet plots. Hydrogen simulations are run with base setting EUR $= 1$, $\kappa = 6 \cdot 10^{-6}$, $\mathrm{EI}_o = 2$ mg (kg fuel)$^{-1}$ and lognormal size distribution with geometric mean radius $\mu_o = 7.5$ nm and geometric width $\sigma_o \approx 1.45$ for lubrication oil droplets. For ambient aerosols we have hygroscopicity parameter $\kappa = 0.5$ and lognormal size distribution with geometric mean radius $\mu_a = 15$ nm and geometric mean width $\sigma_a = 2.2$.

~~To get~~ To gain an improved understanding of how the average contrail EF for hydrogen ~~combustion aircraft depend on the parametrization~~ aircraft depends on the parametrisation of lubrication oil size distributions and other key uncertain-

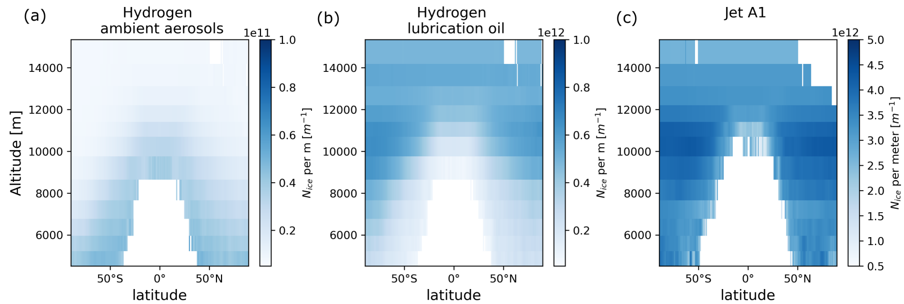

Figure 3. Comparison of average number of ice particles after the vortex downwash per meter ~~between jet and~~ formed by hydrogen ~~contrail cirrus~~ aircraft (~~with ambient aerosol~~ (a) and ~~lubrication oil~~ (b)) and fossil jet fuel aircraft (c). For hydrogen aircraft, the ice particles formed are separated ~~for hydrogen~~into those formed on ambient aerosol (a) ~~after the vortex downwash~~and lubrication oil (b), respectively. Note the difference in scale between all three plots. Hydrogen simulations are run with base setting ~~GI= 55~~EUR = 1, $\kappa = 6 \cdot 10^{-6}$, $\mathrm{EI}_o = 2$ mg (kg fuel)$^{-1}$ and lognormal size distribution ~~LogNormal(~~with geometric mean radius $\mu_o = 7.5$ nm ~~, $\sigma_o \approx 1.45$)~~ and geometric width $\sigma_o \approx 1.45$ for lubrication oil ~~and,~~ droplets. For ambient aerosols we have hygroscopicity parameter $\kappa = 0.5$ and ~~LogNormal(~~lognormal size distribution with geometric mean radius $\mu_a = 15$ nm ~~,~~and geometric mean width $\sigma_a = 2.2$~~) for ambient aerosols~~. All simulations are run for 20 randomly chosen dates (see ~~supplementary~~ Supplement S5) as a representative sample for ~~year~~ 2019.

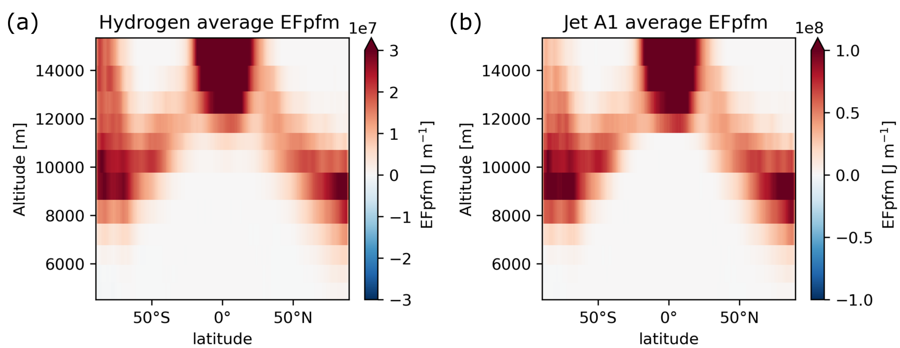

Figure 4. Comparison of average EFpfm between fossil jet fuel aircraft (b) and hydrogen aircraft (~~c~~a)~~persistent contrails~~. Note the difference in scale between the plots. Hydrogen simulations are run with ~~with~~ base setting ~~GI= 55~~EUR = 1, $\kappa = 6 \cdot 10^{-6}$, $\mathrm{EI}_o = 2$ mg (kg fuel)$^{-1}$ and lognormal size distribution ~~, LogNormal(~~with geometric mean radius $\mu_o = 7.5$ nm ~~, $\sigma_o \approx 1.45$),~~ and geometric width $\sigma_o \approx 1.45$ for lubrication oil ~~and,~~ droplets. For ambient aerosols we have hygroscopicity parameter $\kappa = 0.5$ and ~~LogNormal(~~lognormal size distribution with geometric mean radius $\mu_a = 15$ nm ~~,~~and geometric mean width $\sigma_a = 2.2$~~) for ambient aerosols~~.

ties~~we perform~~ , we conducted a sensitivity analysis. In these simulations, ~~we use the same~~ 20 ~~randomly chosen dates (see supplementary~~ dates were chosen randomly (see Supplement S5), for computational cost reasons, as a representative sample for ~~year~~ 2019 ~~for all simulations.~~ (the same days analysed for all cases). Further, averages of contrail cirrus properties are limited to the grid covering latitudes 70°S-70°N, all longitudes and flight levels 300-200 hPa (about 9000-12000 m). However, this region encompasses the airspace in which nearly all commercial flights operate. The ambient aerosol concentration is kept constant at the base setting for all simulations in this section, a sensitivity analysis of ambient aerosol concentration is discussed below and details of that can be found in Supplement S8. For the lubrication oil, we use a span of geometric mean radius μ_o from 5 ranging from 1 nm to 25 nm in steps of 5 nm and the standard deviation and a geometric width σ_o between ranging from $e^{0.25} \approx 1.28$ and to $e^{1.0} \approx 2.72$ in steps of $e^{0.25}$. For these spans of mean and standard deviation we investigate our base settings with We investigate the model sensitivity with respect to the lubrication oil size distribution while keeping our other base case settings intact. For example, lubrication oil hygroscopicity parameter $\kappa_o = 6 \cdot 10^{-4}$, oil droplet mass emission index $\mathrm{EI}_o = 2$ mg (kg fuel)$^{-1}$ and energy consumption ratio ECRusage ratio EUR$= 1$. In addition we test Moreover, we analyse three additional cases 1) with the hygroscopicity parameter changed to $\kappa_o = 0.1$, 2) oil droplet mass emission index $\mathrm{EI}_o = 20$ mg (kg fuel)$^{-1}$ and 3) the Energy consumption ratio ECRenergy usage ratio EUR$= 1.6$. A hygroscopicity parameter as high as of 0.1 is quite unreasonable unreasonably high for lubrication oil but it is assumed so as to better understand the sensitivity improve our understanding about the sensitivity of the model output in relation to our base assumption. One case of oil droplet emission mass index of $\mathrm{EI}_o = 40$ mg (kg fuel)$^{-1}$ was measured in (Yu et al., 2010), although all other values lay in the range 0.1-3 mg (kg fuel)$^{-1}$. A value of $\mathrm{EI}_o = 20$ mg (kg fuel)$^{-1}$ is therefore not out of range but quite extreme. case assumption.

Average energy forcings per flight meter covering latitudes 70°S-70°N, all longitudes and flight levels 300-200 hPa (ca 9000-12000 m)for In Fig. 5 we show the main results from our sensitivity analysis. For all panels, the x-axes show the average number of exhaust particles per contrail generating flight meter N in the 20 dates during 2019 are calculated and shown in the first row simulations (oil droplets for the hydrogen aircraft and soot for the fossil jet fuel aircraft). The average number of oil droplets is determined by μ_o, σ_o and the average fuel flow (which is equal for all cases except EUR$= 1.6$). The smaller the geometric mean radius of the size distribution, the larger the number of oil droplets N for the same EI_o. For each colour (case), the dots appear from left to right in order of decreasing geometric mean radius, with the largest radius on the left and the smallest on the right.

We begin by analysing the first and second rows of Fig. 5, which show the average EFpfm and average N_{ice} pcm, respectively, for all lubrication-oil size distributions and cases. A first observation is that there are a few cases for which hydrogen contrail cirrus have higher EFpfm than contrail cirrus formed by hydrogen aircraft have a higher average EFpfm than those formed by current conventional fossil jet fuel of todayaircraft (jet fuel values from simulations are shown as the black x-marker). This occurs when assuming a high lubrication oil emission intensity EI_o or a high κ, combined with size distribution assumptions with small standard deviation and small mean radius. For high oil emission intensity this is due to the enabling a large number of oil droplets available. Even if the Kelvin effect leads to a smaller share to activate (many droplets but not too small) such as for $\mu_o = 5$nm and $\sigma_o = 1.28$ in panel (a) or $\mu_o = 1$nm and $\sigma_o = 2.12$ in panel (b). A high EI_o provides a larger number of oil droplets activated into ice particles, which can be seen from the smaller increase in ice particles per meter between 10 nm and 5 nm(e), a large number can still be formedthan when using the base case setting, which opens the possibility for more ice particles to form. However, panel (e) in the second row of Fig. 5, showing the average N_{ice} pcm, clearly demonstrates that for the cases with the largest values for N (corresponding to $\mu_o = 1$ nm and $\mu_o = 3$ nm), the Kelvin effect suppresses the fraction of droplets that activate. The high ~~κ has a large impact for small mean radius and variance since it enables a larger share of the droplets available to activate .~~

~~In general we can see in Fig 5 that distributions with small mean radius and variance have larger average EFpfm (see first column and small mean radius). The high EFpfm is seen to drop off quite rapidly as mean radius (follow the x-axis to the right in each panel) and standard deviation are increased (as shown by the different columns) . The high EFpfm for small radius and variance is again due~~ $\kappa_o = 0.1$ enables more oil droplets to ~~the larger number of oil droplets that can activate into water droplets, which can~~ activate compared to the base setting and this causes an increase in N_{ice} pcm and EFpfm for the same N. The highest average EFpfm was obtained for $\mu_o = 3$ nm, $\sigma_o = 1.28$ and $\kappa_o = 0.1$ with a 43% increase compared to fossil jet fuel and a 385% increase compared to the base case in Sec. 4.1. The second highest average EFpfm was obtained for $\mu_o = 1$ nm, $\sigma_o = 1.65$ and $EI_o = 20$ mg (kg fuel)$^{-1}$. For this case, we get a 27% increase in average EFpfm compared to fossil jet fuel and a 330% increase compared to the hydrogen base case.

Further, fossil jet fuel aircraft generate higher average EFpfm and N_{ice} pcm compared to hydrogen aircraft in cases where the number of lubrication oil droplets and soot particles are equal (equal N). This happens despite lower levels of supersaturations in the fossil jet fuel aircraft plume, as compared to the hydrogen aircraft one. The reason is that soot has a higher hygroscopicity and larger particles (approx. $\kappa_s = 0.005$ and $\mu_s = 25$ nm) than is the case for the lubrication oil cases we analyse that generate equal N.

The substantial reduction in average EFpfm and N_{ice} for $\mu_o = 1$ and 3 nm compared to larger geometric mean radii, despite the much larger N shown in panels (a) and (e) respectively, is due both to the suppression of activation by the Kelvin effect and, indirectly, to the omission of the Kelvin effect from the condensation sink formulation. As noted in Sec. 3.1.1, the original and modified K15 models find the quench-time when the supersaturation forcing is equal to the condensation sink. With higher supersaturation values in the plume for hydrogen than fossil fuel aircraft, the condensation sink is increased (L_w is cubic with respect to s_w) and the quenching time decreases. In some cases, this leads to quenching before plume supersaturation becomes sufficiently high to activate the many smaller oil droplets associated with certain size distributions. This behaviour of the K15 model is actually present regardless of fuel and can also lead to shorter quench-times for colder ambient temperatures. In general colder ambient temperatures generate higher supersaturations in the plume, leading to an increase in condensation sink and shorter quench-times. This mechanism–e.i., high supersaturation with increased condensation sink leading to short quench-times–can also be seen in ~~the second row as ice particles per meter after downwash. Since the ice water content of the plume~~ Fig. 1 in ambient aerosol activation, where cold ambient temperatures give a lower percentage of entrained and activated particles because of quenching before full entrainment. This mechanism is also visible in panel (c) of Fig. 2 in Bier and Burkhardt (2019) for ambient aerosols (in combination with soot), where plume quenching occurs in less time than is needed for full entrainment and activation, leading to fewer ice particles formed from ambient aerosols for colder ambient temperatures. Both these examples are contrast with the increase in ice particles formed (from ambient aerosols) at lower ambient temperatures in Bier et al. (2024), which does not include a quenching procedure. The only study investigating this feature of the K15 model is Ponsonby et al. (2025), which found an underestimation of 10-30% of formed ice particles compared to the modified pyrcel model for radii $1-4$ nm and hygroscopicity $0-0.5$ in the soot-poor regime ($EI_{soot} < 10^{13}$

(kg fuel)$^{-1}$). We might therefore expect N_{ice} to be underestimated, especially for oil droplet distributions with small geometric mean radii and small geometric widths.

We next turn to the third row of Fig. 5, which shows the average contrail lifetime for all lubrication-oil size distributions and cases. The ice water content in the plume is the same for all cases ~~, except the case with higher ECR, is the same and that in CoCiP, this~~ with the hydrogen aircraft, except for the one with a higher EUR. In CoCiP, the ice water content is assumed to be shared equally among the ~~particles formed, more particles lead to smaller particles~~ droplets activated. Therefore, a larger number of activated droplets leads to smaller ice particles, as noted in Sec. 4.1~~and seen in the last row of Fig. 5 where we show ice particle radius averaged over contrail cirrus lifetime.~~. Smaller average particles sediment ~~more slowly and thereby~~ slower and thereby generally give longer contrail cirrus average lifetimes~~in general~~, as can be seen in row three of Fig. 5. There are exceptions to this, ~~since evaporation~~ as sublimation also plays a role in contrail cirrus lifetime. ~~We cansee this for the high lubrication oil emission case where the contrail cirrus lifetime is seen to be lower for $\mu_o = 5$ nm in comparison to $\mu_o = 10$ nm for small σ_o ((i) and (j)). Here the ice particles are small enough that evaporation shortens the contrail cirrus average lifespan~~This can, for example, be seen for $\sigma_o = 1.65$ in panel (j), where contrail cirrus lifetimes are shorter for $\mu_o = 1$ nm than for $\mu_o = 3$ nm, despite their larger average N_{ice} pcm in panel (f) of row two.

In ~~row four~~ rows four and five of Fig. 5, we show the optical depth ~~averaged over~~ and the ice particle radius, respectively, averaged over the contrail cirrus lifetime for all cases. ~~We see that, in generalthe high ice particle number cases also lead to high~~ In general, the optical depth follows the average N_{ice} pcm, while the average ice particle radius varies inversely. Higher N_{ice} pcm leads to smaller r_{ice}, which in turn results in higher optical depth. ~~A noticeable break in this trend is the lower optical depth for fossil jet fuel compared to high oil emission and high κ for $\sigma \approx 1.28$ despite a larger number of ice particles per meter after downwash~~Conversely, lower N_{ice} pcm leads to larger r_{ice} and therefore lower optical depth.

We next compare cases with the base EI_o and with a tenfold increase in EI_o that produce the same number of lubrication-oil droplets in the plume, N, but differ in size distribution. Under these conditions, EFpfm remains higher for the larger EI_o, owing to the shift in size distribution toward larger droplets when more oil is available to form the same number of droplets. This shift leads to an increase in the share of particles in the exhausts that are activated. Furthermore, this mechanism is more important for smaller particles that are less likely to activate than larger particles. For small μ_o, the tenfold increase in EI_o leads to an approximate 90-250% increase in EFpfm, whereas for the largest comparable geometric mean radius, $\mu_o = 10$ nm, the increase is only about 5-10%. Size distributions with $\mu_o > 10$ nm in the base EI_o setting all produce fewer droplets than any of the size distributions in the increased-EI_o cases.

In Fig. 6, we show the average EFpfm but with the geometric mean radius for lubrication oil droplets on the x-axis. Shown in this way we can see that an increase in EI_o, with an associated increase in available oil droplets with the same size distribution leads to a higher average EFpfm. In general, there is a 22-450% increase of average EFpfm (depending on size distribution) for our tenfold increase in EI_o. The smallest increase in EFpfm is found for the case with widest distribution and geometric mean radius of 25 nm. The largest increase was obtained for a geometric mean radius of 20 nm and geometric width of 1.28.

It is also interesting that the ~~assumptions of technical proficiency (GI, fuel flow and ECR) have a rather~~ assumption about a lower fuel efficiency (EUR is 60% higher) only has a modest effect in comparison to the oil droplet mass emission index.

The increase in EFpfm is smaller than ~~1.6 for the lower gravimetric index~~the 60% increase in fuel flow. This is partly due to the larger ice water content for the higher ~~ECR~~ EUR leading to proportionally larger ice particle losses in the wake vortex downwash of CoCiP.

4.2.1 ~~Ambient Aerosol contribution to ice particle formation~~

4.3 Ambient aerosol contribution to ice particle formation

The contribution of ambient aerosols to ~~the formation of ice particles in absolute numbers varies slightly depending on the size distribution and amount of oil droplets. For a large amount~~ ice particle formation, in absolute terms, is nearly constant across the different oil droplet size distributions and number concentrations considered here. This is because the quench time, which determines the level of entrainment, is controlled primarily by the supersaturation forcing and the condensation sink, as discussed in Sec. 4.2.1. However, the lubrication-oil size distribution does exert some influence on the contribution from ambient aerosols. When large numbers of oil droplets ~~present, the droplets quickly~~ are present, they deplete the available water ~~and "quench " the plume leaving little time~~ more rapidly and quench the plume sooner, thereby reducing the time available for ambient aerosols to be entrained into the plume and contribute to ice particle formation. For such cases, both the relative share of ice particles formed on ambient aerosols and ~~absolute number are smaller although~~ the absolute number ~~marginally so. In fact ice particles from ambient aerosols is almost the same magnitude for all cases~~ is smaller than for cases in which a small number of oil droplets is present, as seen in Fig. 7, ~~where~~ in which we show the average numbers of ice particles from ~~lubrication oil (b) and~~ ambient aerosols (a) ~~after downwash~~ and lubrication oil (b) after downwash, as well as the ambient aerosol ice particle number as a percentage (c) for all cases and size distributions ~~. In~~ examined in the sensitivity analysis. The decrease in the case with smallest $N_{ice,a}$ compared to the case with the largest $N_{ice,a}$ is only 4%. This implies that in cases where there are few~~er~~oil droplets present at formation, the ambient aerosols ~~contribute with a larger share and in the case with oil size distributions with large means and variances the ambient aerosols~~ are responsible for the majority of ice particles ~~.~~

~~The~~ as seen in Fig. 7 panel (c). This explains the "plateauing" of N_{ice} and EFpfm seen in panels (d) and (h) in Fig. 5, where the ambient aerosol contribution background value is reached. This is the end point of our ranges with $\mu_o = 25$ nm and $\sigma_o \approx 2.72$, which gives the lowest number of oil particles~~, can be seen as a rough estimate of the average EFpfm for ambient aerosols alone (an exception isthe case when we assume a high oil emission index).~~. The ambient aerosol contribution background value can be considered the best case in terms of contrail cirrus climate impact from hydrogen aviation. It is approximately what the average EFpfm would be if the contribution from lubrication oil were to be eliminated.

We analyse the consequences of both increasing and decreasing the ambient aerosol number concentration by a factor of ten for a subset of oil droplet size distributions spanning the range considered in Sec. 4.2.1; see Supplement S8. In general, the larger the fraction of ice particles formed on ambient aerosols under our base-case aerosol concentration, the larger the corresponding increase or decrease in average EFpfm following a tenfold increase or decrease in ambient aerosol concentration, respectively. The strongest sensitivity is found for cases in which nearly all ice particles form on ambient aerosols, that is, where the ambient-aerosol background contribution dominates. For the lubrication-oil parameters with the lowest fraction of ice particles formed on oil droplets, 2% ($\mu_o = 25$ nm and $sigma_o \approx 2.72$), we obtain a 620% increase in average EFpfm for a tenfold increase in ambient aerosol number concentration, and a 90% decrease for a tenfold decrease in concentration. Even in this case, however, the average EFpfm with a tenfold increase in ambient aerosol concentration remains 44% lower than in the overall hydrogen base case. It is also 90% lower than the average EFpfm for fossil jet fuel aircraft.

5 Discussion

Our analysis of ~~contrail cirrus impacts of hydrogen as aviation fuel~~ how hydrogen as a jet fuel impacts contrail cirrus formation and energy forcing indicates the possibility of a significant climate benefit. For almost all parameter settings considered, we find that hydrogen offers a reduction in energy forcing per flight meter compared to conventional ~~jet~~ fossil jet fuel aircraft, with a global average reduction of ~~about 70%~~ 66% when using our base case assumptions. ~~For~~ In our base case, we find an average ice particle reduction of approximately 85% compared to ~~conventional jet while a reduction of more than~~ a conventional fossil jet fuel aircraft. This can be compared to previous estimates of a reduction exceeding 80-90%~~was found in (Bier et al., 2024) for hydrogen combustion with~~ , although only ambient aerosols were considered as ice nuclei ~~. One may further note that SAF is expected to reduce the number of ice particles. One study found a 49% reduction for 100% SAF (Teoh et al., 2022b). However~~in that study (Bier et al., 2024). In our study, the ice particle number ~~in our study,~~ is highly dependent on the lubrication oil size distribution and ~~lubrication oil emission index. We find a few percent of reduction in the worst case of~~ less (but still significantly) dependent on lubrication oil mass emission index and lubrication oil hygroscopicity. In our most pessimistic cases, we find an increase of about 10% in the ice particle number after downwash, relative to the case for a conventional fossil jet fuel aircraft, assuming a high oil emission index ~~and~~ or high hygroscopicity, combined with a small lubrication oil geometric mean radius and a small ~~standard deviation for~~ geometric width. However, we found a 99% reduction in the ice particle number after downwash ~~, but up to around 99% reduction for larger oil dropletswhen~~ when assuming relatively large lubrication oil droplets, corresponding to a situation in which lubrication oil is vented rather than emitted in the main exhaust. This ~~shows~~ indicates the possibilities and importance of future hydrogen ~~engines design~~ engine designs for a low contrail cirrus climate impact.

~~Despite the reduction in the majority of cases there are~~ Although the simulated reductions in ice particle number and energy forcing are robust across nearly all cases investigated here, uncertainties and caveats in the modelling approach ~~used~~must still be taken into account. CoCiP is a simplified model ~~and~~ although it has been calibrated and compared (with a relatively good fit) against data (Schumann et al., 2017)~~, these data are mainly from the middle part of the contrail cirrus life-time and the comparison might therefore not capture the full effect of the contrail cirrus. A~~ . However, a recent comparison between CoCiP and APCEMM (Akhtar Martínez et al., 2025) highlights the fact that a substantial part of the contrail cirrus~~later life-time~~ ' later lifetime might be missed in the CoCiP model. This leads to a lower estimate of the life-time optical depth (proxy for climate impact) in CoCiP compared to APCEMM~~by approximately a factor 4.~~ , by an approximate factor of 4 for fossil jet fuel.

~~For APCEMM a large part of the life-time optical depth in the model comes from the latest stages of contrail cirrus life-time which is hard to measure with various instruments due to low optical depth. It is still uncertain if APCEMM or CoCiP is closer~~

~~to the real world. However, APCEMM fall-streak behaviour is largely in agreement with more resolved models than CoCiP (Unterstrasser and Gierens, 2010; Lewellen et al., 2014; Lewellen, 2014).~~

~~If contrail cirrus lifespan is modelled to be too short in CoCiP the most affected contrail cirrus would be those with high initial ice water content and low ice particle numbers which, in the model, generate large ice particles with a fast sedimentation. Since CoCiP does not employ sizedistributions, all particles~~ The modelling approach in CoCiP does not employ size distributions of ice particles in the plume. Since the sedimentation rate depends on particle size, all ice particles in CoCiP sediment at the same rate, with the consequence that a ~~longer lived~~ longer-lived tail of smaller particles ~~are missed. Since high~~ would be missed. In the model, the contrail cirrus with high initial ice water content and ~~fewer particles at formation is possible for hydrogen combustion, there is a risk of a relatively larger underestimation of~~ low ice particle numbers will generate large ice particles with rapid sedimentation. However, it remains unclear whether such cases would lead to a greater relative underestimation of contrail lifetime and energy forcing per ~~meter for hydrogen (for cases with broader distributions with larger mean radii in our study) than for fossil jet fuel in CoCiP.~~ flight meter because of the omitted longer-lived tail, or whether such a tail would in fact be less pronounced in cases that initially contain only a small number of large particles, potentially making CoCiP more representative in those situations.

~~From the~~ For APCEMM, a large part of the lifetime optical depth in the model comes from the latest stages of contrail cirrus lifetime. This may explain the discrepancy between the models according to (Akhtar Martínez et al., 2025). Due to a low optical depth in the later stages, this phase of contrail cirrus lifetime is difficult to measure and therefore makes it difficult to validate model results against data. Measurement difficulties notwithstanding, APCEMM sedimentation behaviour is largely in agreement with more resolved models than CoCiP (Unterstrasser and Gierens, 2010; Lewellen et al., 2014; Lewellen, 2014).

The theoretical K15 model in (Kärcher et al., 2015) for ice particle formation ~~we expect an overestimation~~ is expected, on the one hand, to overestimate the number of ice particles due to the ~~"quench "-procedure where~~ quench procedure, in which all water droplets form at once rather than as a successive activation of particles into water droplets. A successive activation would ~~successively~~ steadily deplete the supersaturation, thus ~~lowering it under~~ taking it below the activation threshold for small particles and particles with low hygroscopicity.

~~The magnitude of overestimation due to the~~ On the other hand, the formulation of the condensation sink may lead to an underestimation of the number of formed ice particles, especially for small droplets affected by the Kelvin effect. When comparing a modified version of K15 ~~model and the~~ with a modified version of the pyrcel model, K15 generated approximately 10-30% lower ice particle numbers for radii $1-4$ nm and hygroscopicity $0-0.5$ in the "soot-poor" regime for kerosene combustion (Ponsonby et al., 2025). How this translates to hydrogen combustion is not clear and needs to be studied explicitly. However, given the higher supersaturation and supersaturation forcing in the plume for hydrogen combustion, we suspect this mechanism could further enhance the underestimation because of ~~possibly shorter lifespan due to the modelling approach in CoCiP~~ the cubic dependence of the condensation sink to supersaturation in the K15 model, although this remains to be tested.

Due to our modelling approach, the magnitude of the uncertainties of contrail cirrus impact is difficult to estimate. There are no observations, as yet, of ice particle formation from hydrogen ~~flight yet~~ flights against which to compare our ice particle estimates . Althoughand contrail evolution. However, the first measurement campaign of contrail formation from hydrogen aircraft was launched in December 2024 and with its upcoming publication we can better understand the modelling caveats. As mentioned above the latest stages of contrail cirrus life-time is largely unmeasured due to low optical depth.

An interesting finding in our study is the relatively small difference in EF per flight meter between our base case and the more technically pessimistic assumption of a lower gravimetric index with an increase in energy usage by a factor of 1.6. It is also worth noting that if our base case hygroscopicity underestimates the actual hygroscopicity of lubrication oil or if there are versions with higher κ, this would not increase the climate impact to any significant degree. The prominent factor, is the amount of particles present for ice particle formation, as shown in Still, our modelling approach produces ice particle numbers of the same order of magnitude as those reported in another study for comparable lubrication-oil size distributions and emission indices (Zink et al., 2025b). We also obtain relatively lower numbers of formed ice particles for smaller geometric mean radii, consistent with the tendency of K15 to relatively underestimate ice particle numbers when small geometric mean radii are assumed for the condensation nuclei, as noted in (Ponsonby et al., 2025). A more precise comparison is hampered by modelling differences. For example, we estimate the global annual average ice particle numbers after downwash (with realistic meteorology), compared to ice particle numbers before downwash at four different temperatures (Zink et al., 2025b).

In general, EFpfm increases with the number of exhausts particles (oil droplets), but this trend reverses for very high numbers of droplets (see Fig. 5 in terms of emission index and lubrication oil size distribution. Although there is asaturation effect, as seen with the higher lubrication oil emission index for small radii and narrow distributions, that could be alleviated with more favourable circumstances for activation with higher ECR or higher hygroscopicity. In general though, an increase in ice water content as with low gravimetric index, high hygroscopicity and to some extent smaller particles have a smaller effect than the number of particles that can act as condensation nucleipanel (a)). This reversal arises because, in our study, very high droplet numbers correspond to small droplets, for which activation is suppressed by the Kelvin effect. For the smallest geometric width, this generates an almost exponential decrease in EFpfm with increasing N for oil droplet numbers approximately $N > 10^{13}$ m^{-1}, corresponding to geometric mean radii of < 5 nm. This is the fraction of the parameter space in which we expect the largest underestimation of ice particles formed. For the largest geometric width tested with a significant number of large droplets, EFpfm increases approximately exponentially with N, for $N > 10^{10}$ m^{-1}.

As the main determining factor for the magnitude of energy forcing per meter is Following a tenfold increase in the emission index, the increase in EFpfm is highly dependent on oil droplet size distribution. We find the increase to be in the range 22-450%, with the smallest value for geometric mean radius of 25 nm and a geometric width of 2.72 and the largest increase for a geometric mean radius of 20 nm and geometric width of 1.28. An additional finding in our study is the amount of particles present for ice particle formation rather than the properties of the particles, it indicates that our simplified approach to handle ambient aerosols is good enough for the purpose of the study. We assumed that the ambient aerosols could be described by single lognormal distribution using a single hygroscopicity. We intentionally did set the relatively small difference in EFpfm between our base case and the more technically pessimistic assumption for fuel systems.

The best cases in terms of lowest contrail cirrus energy forcing are obtained for particle size distributions generating approximately $N < 10^{10}$ m^{-1} and large droplets. Here, ambient aerosols dominate the ice particle formation. In the modelling, we have set the constant ambient aerosol concentration relatively high and assumed a relatively high hygroscopicity value so that the ice particle contributionfrom ambient aerosols are at the high end.

However, there are locations where the concentration is even higher measuring up to 15000 cm^{-3} in the upper troposphere of the northern hemisphere for ultrafine particles with radii $<$ 5 nm (Minikin et al., 2003). This, however, is in general a local occurrence and high ice particle numbers would be hindered to some degree by the Kelvin effect in activationto avoid underestimation of their contribution. We also varied the ambient aerosol concentration by an order of magnitude upward and downward. The effect of this change is greatest in cases that otherwise have relatively low energy forcing. Even with a tenfold increase in ambient aerosol concentration relative to our base-case assumption, the average EFpfm remains 90% lower than for fossil jet fuel in the case with the smallest contribution of lubrication oil to the ice particle number.

Despite the uncertainties, our study indicates the possibility of substantial climate benefits in terms of reduced contrail cirrus EF per flight meter for hydrogen in comparison EFpfm for hydrogen compared to conventional jet . In addition, our fuel. Our parameter sweep over the lubrication oil size distributions give may also provide guidance for future hydrogen engine design. Releasing lubrication oil in the main exhaust at high temperatures should be avoided and there is a potentially large climate benefit in more efficient recapturing schemes and venting (if necessary) as far away from the exhaust as possible to minimize entrainment into the plumeFrom a contrail cirrus climate impact perspective, if mass emission index of entrained lubrication oil remains unchanged, a broad size distribution with a large geometric mean radius is preferable.

6 Conclusions

Our results indicate that in the majority of settings we analysed, contrail cirrus from hydrogen combustion aircraft generate generates a significantly lower energy forcing than those that from fossil jet fuel combustion under a majority of settingsaircraft. The primary mechanism is a reduced number of particles available to act as ice nuclei. While fossil jet fuel combustion emits soot and other volatile particulate matter particulates that dominate ice nucleation, contrail formation from hydrogen combustion depends instead on lubrication oil particles droplets and ambient aerosols serving as condensation nuclei.

We show that In our modelling approach ice particle formation on lubrication oil and ambient aerosols can be is captured using activation emulators based on a modified version of the microphysical framework proposed by Kärcher et al. (Kärcher et al., 2015). Although lubrication oil may partially compensate for the absence of soot, its effectiveness as an ice nucleus is highly sensitive to poorly constrained factors such as its emission index and particle size distribution. Nonetheless, the conclusion that hydrogen combustion leads to lower contrail cirrus energy forcing remains robust intact across a wide range of assumptions regarding lubrication oil properties.

Overall, our findings suggest that hydrogen aircraft may offer not only CO_2-free propulsion but also substantially reduced non-CO_2 climate impacts from contrail cirrus, provided that lubrication oil emissions are effectively controlled. Engine design should therefore treat lubrication oil handling as a critical parameter.

Code and data availability. Contrail model codes and generated data are available for scientific research purposes from the authors upon request and partly found at https://doi.org/10.5281/zenodo.15874256.

Author contributions. SP and DJ designed the study. SP carried out the simulations, analysis and the preparation of the manuscript. DJ helped with the analysis. DJ and CA contributed to the preparation of the manuscript.

Competing interests. The authors declare no conflict of interests.

Acknowledgements. Funding has been provided by VINNOVA grant number 2023-01286, Chalmers Area of Advance Transport.

References

Adler, E. J. and Martins, J. R.: Hydrogen-powered aircraft: Fundamental concepts, key technologies, and environmental impacts, Progress in Aerospace Sciences, 141, 100 922, 2023.

Akhtar Martínez, C., Eastham, S. D., and Jarrett, J. P.: Contrail models lacking post-fallstreak behavior could underpredict lifetime optical depth, EGUsphere, 2025, 1–26, 2025.

Bier, A. and Burkhardt, U.: Variability in contrail ice nucleation and its dependence on soot number emissions, Journal of Geophysical Research: Atmospheres, 124, 3384–3400, 2019.

Bier, A., Unterstrasser, S., Zink, J., Hillenbrand, D., Jurkat-Witschas, T., and Lottermoser, A.: Contrail formation on ambient aerosol particles for aircraft with hydrogen combustion: a box model trajectory study, Atmospheric Chemistry and Physics, 24, 2319–2344, 2024.

Borrmann, S., Kunkel, D., Weigel, R., Minikin, A., Deshler, T., Wilson, J. C., Curtius, J., Volk, C. M., Homan, C. D., and Ulanovsky, A.: Aerosols in the tropical and subtropical UT/LS: in-situ measurements of submicron particle abundance and volatility, Atmospheric Chemistry and Physics, 10, 5573–5592, 2010.

Clarke, A. D. and Kapustin, V. N.: A Pacific aerosol survey. Part I: A decade of data on particle production, transport, evolution, and mixing in the troposphere, Journal of the atmospheric sciences, 59, 363–382, 2002.

Decker, Z. C., Alpert, P. A., Ammann, M., Anet, J. G., Bauer, M., Cui, T., Durdina, L., Edebeli, J., Gysel-Beer, M., and Pre´voˆt, A. S.: Emission and Formation of Aircraft Engine Oil Ultrafine Particles, ACS EST Air, 1, 1662–1672, 2024.

DLR: World-first in-flight measurements of contrails from hydrogen propulsion, https://www.dlr.de/en/latest/news/2025/world-first-in-flight-measurements-of-contrails-from-hydrogen-propulsion, 2025.

Durdina, L., Brem, B. T., Elser, M., Scho¨nenberger, D., Siegerist, F., and Anet, J. G.: Reduction of nonvolatile particulate matter emissions of a commercial turbofan engine at the ground level from the use of a sustainable aviation fuel blend, Environmental Science Technology, 55, 14 576–14 585, 2021.

Engberg, Z., Teoh, R., Abbott, T., Dean, T., Stettler, M. E., and Shapiro, M. L.: Forecasting contrail climate forcing for flight planning and air traffic management applications: the CocipGrid model in pycontrails 0.51. 0, Geoscientific Model Development, 18, 253–286, 2025.

Fritz, T. M., Eastham, S. D., Speth, R. L., and Barrett, S. R. H.: The role of plume-scale processes in long-term impacts of aircraft emissions, Atmos. Chem. Phys., 20, 5697–5727, https://doi.org/10.5194/acp-20-5697-2020, 2020.

Fushimi, A., Saitoh, K., Fujitani, Y., and Takegawa, N.: Identification of jet lubrication oil as a major component of aircraft exhaust nanoparticles, Atmospheric Chemistry and Physics, 19, 6389–6399, 2019.

Gierens, K., Matthes, S., and Rohs, S.: How well can persistent contrails be predicted?, Aerospace, 7, 169, 2020.

Hersbach, H., Bell, B., Berrisford, P., Hirahara, S., Horányi, A., Muñoz-Sabater, J., Nicolas, J., Peubey, C., Radu, R., and Schepers, D.: The ERA5 global reanalysis, Quarterly journal of the royal meteorological society, 146, 1999–2049, 2020.

Kaiser, J. C., Hendricks, J., Righi, M., Jöckel, P., Tost, H., Kandler, K., Weinzierl, B., Sauer, D., Heimerl, K., and Schwarz, J. P.: Global aerosol modeling with MADE3 (v3. 0) in EMAC (based on v2. 53): model description and evaluation, Geoscientific Model Development, 12, 541–579, 2019.

Kärcher, B.: The importance of contrail ice formation for mitigating the climate impact of aviation, Journal of Geophysical Research: Atmospheres, 121, 3497–3505, 2016.

Kärcher, B. and Yu, F.: Role of aircraft soot emissions in contrail formation, Geophysical Research Letters, 36, 2009.

Kärcher, B., Turco, R., Yu, F., Danilin, M., Weisenstein, D., Miake-Lye, R., and Busen, R.: A unified model for ultrafine aircraft particle emissions, Journal of Geophysical Research: Atmospheres, 105, 29 379–29 386, 2000.

Kärcher, B., Burkhardt, U., Bier, A., Bock, L., and Ford, I.: The microphysical pathway to contrail formation, Journal of Geophysical Research: Atmospheres, 120, 7893–7927, 2015.

Kölker, K., Zengerling, Z., Kühlen, M., Lütjens, K., and Linke, F.: Assessing the impact of contrail avoidance through rescheduling on airline network flows: A case study of North Atlantic flights, Transportation Research Part A: Policy and Practice, 187, 104 155, 2024.

Lambe, A., Onasch, T., Massoli, P., Croasdale, D., Wright, J., Ahern, A., Williams, L., Worsnop, D., Brune, W., and Davidovits, P.: Laboratory studies of the chemical composition and cloud condensation nuclei (CCN) activity of secondary organic aerosol (SOA) and oxidized primary organic aerosol (OPOA), Atmospheric Chemistry and Physics, 11, 8913–8928, 2011.

Lee, D. S., Fahey, D. W., Skowron, A., Allen, M. R., Burkhardt, U., Chen, Q., Doherty, S. J., Freeman, S., Forster, P. M., and Fuglestvedt, J.: The contribution of global aviation to anthropogenic climate forcing for 2000 to 2018, Atmospheric Environment, 244, 117 834, 2021.

Lewellen, D.: Persistent contrails and contrail cirrus. Part II: Full lifetime behavior, Journal of the Atmospheric Sciences, 71, 4420–4438, 2014.

Lewellen, D., Meza, O., and Huebsch, W.: Persistent contrails and contrail cirrus. Part I: Large-eddy simulations from inception to demise, Journal of the Atmospheric Sciences, 71, 4399–4419, 2014.

Lewellen, D. C.: A large-eddy simulation study of contrail ice number formation, Journal of the Atmospheric Sciences, 77, 2585–2604, 2020.

Liu, H., Zhao, C., Nekat, B., Ma, N., Wiedensohler, A., Van Pinxteren, D., Spindler, G., Müller, K., and Herrmann, H.: Aerosol hygroscopicity derived from size-segregated chemical composition and its parameterization in the North China Plain, Atmospheric Chemistry and Physics, 14, 2525–2539, 2014.

Minikin, A., Petzold, A., Ström, J., Krejci, R., Seifert, M., van Velthoven, P., Schlager, H., and Schumann, U.: Aircraft observations of the upper tropospheric fine particle aerosol in the Northern and Southern Hemispheres at midlatitudes, Geophysical Research Letters, 30, 2003.

Moore, R. H., Thornhill, K. L., Weinzierl, B., Sauer, D., D'Ascoli, E., Kim, J., Lichtenstern, M., Scheibe, M., Beaton, B., and Beyersdorf, A. J.: Biofuel blending reduces particle emissions from aircraft engines at cruise conditions, Nature, 543, 411–415, 2017.

Mukhopadhaya, J. and Rutherford, D.: Performance analysis of evolutionary hydrogen-powered aircraft, ICCT white paper, 2022.

Nuic, A., Poles, D., and Mouillet, V.: BADA: An advanced aircraft performance model for present and future ATM systems, International journal of adaptive control and signal processing, 24, 850–866, 2010.

Padró, L. T., Tkacik, D., Lathem, T., Hennigan, C. J., Sullivan, A. P., Weber, R. J., Huey, L. G., and Nenes, A.: Investigation of cloud condensation nuclei properties and droplet growth kinetics of the water-soluble aerosol fraction in Mexico City, Journal of Geophysical Research: Atmospheres, 115, 2010.

Petters, M. and Kreidenweis, S.: A single parameter representation of hygroscopic growth and cloud condensation nucleus activity, Atmospheric Chemistry and Physics, 7, 1961–1971, 2007.

Poll, D. and Schumann, U.: An estimation method for the fuel burn and other performance characteristics of civil transport aircraft in the cruise. Part 1 fundamental quantities and governing relations for a general atmosphere, The Aeronautical Journal, 125, 257–295, 2021a.

Poll, D. and Schumann, U.: An estimation method for the fuel burn and other performance characteristics of civil transport aircraft during cruise: part 2, determining the aircraft's characteristic parameters, The Aeronautical Journal, 125, 296–340, 2021b.

Poll, D. and Schumann, U.: An estimation method for the fuel burn and other performance characteristics of civil transport aircraft; part 3 full flight profile when the trajectory is specified, The Aeronautical Journal, pp. 1–37, 2025.

Ponsonby, J., King, L., Murray, B. J., and Stettler, M. E.: Jet aircraft lubrication oil droplets as contrail ice-forming particles, Atmospheric Chemistry and Physics, 24, 2045–2058, 2024.

Ponsonby, J., Teoh, R., Kärcher, B., and Stettler, M. E.: An updated microphysical model for particle activation in contrails: the role of volatile plume particles, Atmospheric Chemistry and Physics, 25, 18 617–18 637, 2025.

Quante, G., Voigt, C., and Kaltschmitt, M.: Targeted use of paraffinic kerosene: Potentials and implications, Atmospheric Environment: X, p. 100279, 2024.

Raes, F., Van Dingenen, R., Vignati, E., Wilson, J., Putaud, J.-P., Seinfeld, J. H., and Adams, P.: Formation and cycling of aerosols in the global troposphere, Atmospheric environment, 34, 4215–4240, 2000.

Reutter, P., Neis, P., Rohs, S., and Sauvage, B.: Ice supersaturated regions: properties and validation of ERA-Interim reanalysis with IAGOS in situ water vapour measurements, Atmospheric chemistry and physics, 20, 787–804, 2020.

Righi, M., Hendricks, J., and Sausen, R.: The global impact of the transport sectors on atmospheric aerosol: simulations for year 2000 emissions, Atmospheric Chemistry and Physics, 13, 9939–9970, 2013.

Rosenow, J. and Fricke, H.: Luchkova et al. Minimizing contrail formation by rerouting around dynamic ice-supersaturated regions, Aeron Aero Open Access J, 2, 105–111, 2018.

Rädel, G. and Shine, K. P.: Validating ECMWF forecasts for the occurrence of ice supersaturation using visual observations of persistent contrails and radiosonde measurements over England, Quarterly Journal of the Royal Meteorological Society, 136, 1723–1732, 2010.

Schumann, U.: On conditions for contrail formation from aircraft exhausts, Meteorologische Zeitschrift, 5, 4–23, 1996.

Schumann, U.: A contrail cirrus prediction model, Geoscientific Model Development, 5, 543–580, 2012.

Schumann, U., Mayer, B., Gierens, K., Unterstrasser, S., Jessberger, P., Petzold, A., Voigt, C., and Gayet, J.-F.: Effective radius of ice particles in cirrus and contrails, Journal of the Atmospheric Sciences, 68, 300–321, 2011.

Schumann, U., Mayer, B., Graf, K., and Mannstein, H.: A parametric radiative forcing model for contrail cirrus, Journal of Applied Meteorology and Climatology, 51, 1391–1406, 2012.

Schumann, U., Baumann, R., Baumgardner, D., Bedka, S. T., Duda, D. P., Freudenthaler, V., Gayet, J.-F., Heymsfield, A. J., Minnis, P., and Quante, M.: Properties of individual contrails: a compilation of observations and some comparisons, Atmospheric Chemistry and Physics, 17, 403–438, 2017.

Shapiro, M., Engberg, Z., Teoh, R., and Dean, T.: pycontrails: Python library for modeling aviation climate impacts, Zenodo, 2023.

Stier, P., Feichter, J., Kinne, S., Kloster, S., Vignati, E., Wilson, J., Ganzeveld, L., Tegen, I., Werner, M., and Balkanski, Y.: The aerosol-climate model ECHAM5-HAM, Atmospheric Chemistry and Physics, 5, 1125–1156, 2005.

Teoh, R., Schumann, U., Gryspeerdt, E., Shapiro, M., Molloy, J., Koudis, G., Voigt, C., and Stettler, M.: Aviation contrail climate effects in the North Atlantic from 2016–2021, 2022a.

Teoh, R., Schumann, U., Voigt, C., Schripp, T., Shapiro, M., Engberg, Z., Molloy, J., Koudis, G., and Stettler, M. E.: Targeted use of sustainable aviation fuel to maximize climate benefits, Environmental Science Technology, 56, 17 246–17 255, 2022b.

Timko, M. T., Albo, S. E., Onasch, T. B., Fortner, E. C., Yu, Z., Miake-Lye, R. C., Canagaratna, M. R., Ng, N. L., and Worsnop, D. R.: Composition and sources of the organic particle emissions from aircraft engines, Aerosol Science and Technology, 48, 61–73, 2014.

Ungeheuer, F., Caudillo, L., Ditas, F., Simon, M., van Pinxteren, D., Kılıç, D., Rose, D., Jacobi, S., Kürten, A., and Curtius, J.: Nucleation of jet engine oil vapours is a large source of aviation-related ultrafine particles, Communications Earth Environment, 3, 319, 2022.

Unterstrasser, S. and Gierens, K.: Numerical simulations of contrail-to-cirrus transition–Part 1: An extensive parametric study, Atmospheric Chemistry and Physics, 10, 2017–2036, 2010.

Voigt, C., Schumann, U., Jurkat, T., Schäuble, D., Schlager, H., Petzold, A., Gayet, J. F., Krämer, M., Schneider, J., Borrmann, S., Schmale, J., Jessberger, P., Hamburger, T., Lichtenstern, M., Scheibe, M., Gourbeyre, C., Meyer, J., Kübbeler, M., Frey, W., Kalesse, H., Butler, T., Lawrence, M. G., Holzäpfel, F., Arnold, F., Wendisch, M., Döpelheuer, A., Gottschaldt, K., Baumann, R., Zöger, M., Sölch, I., Rautenhaus, M., and Dörnbrack, A.: In-situ observations of young contrails – overview and selected results from the CONCERT campaign, Atmos. Chem. Phys., 10, 9039–9056, https://doi.org/10.5194/acp-10-9039-2010, 2010.

Voigt, C., Kleine, J., Sauer, D., Moore, R. H., Bräuer, T., Le Clercq, P., Kaufmann, S., Scheibe, M., Jurkat-Witschas, T., and Aigner, M.: Cleaner burning aviation fuels can reduce contrail cloudiness, Communications Earth Environment, 2, 114, 2021.

Voigt, C., Märkl, R., Sauer, D., Dischl, R., Renard, C., Seeliger, K., Yu, F., Kaufmann, S., Bräuer, T., and Jurkat-Witschas, T.: Substantial aircraft contrail formation at low soot emission levels, Nature, 652, 112–118, 2026.

Wang, M., Kong, W., Marten, R., He, X.-C., Chen, D., Pfeifer, J., Heitto, A., Kontkanen, J., Dada, L., and Kürten, A.: Rapid growth of new atmospheric particles by nitric acid and ammonia condensation, Nature, 581, 184–189, 2020.

Yang, P., Hong, G., Dessler, A. E., Ou, S. S., Liou, K.-N., Minnis, P., and Harshvardhan: Contrails and induced cirrus: Optics and radiation, Bulletin of the American Meteorological Society, 91, 473–478, 2010.

Yu, F. and Turco, R. P.: The role of ions in the formation and evolution of particles in aircraft plumes, Geophysical Research Letters, 24, 1927–1930, 1997.

Yu, F., Turco, R. P., and Kärcher, B.: The possible role of organics in the formation and evolution of ultrafine aircraft particles, Journal of Geophysical Research: Atmospheres, 104, 4079–4087, 1999.

Yu, F., Karcher, B., and Anderson, B. E.: Revisiting contrail ice formation: Impact of primary soot particle sizes and contribution of volatile particles, Environmental Science Technology, 2024.

Yu, Z., Liscinsky, D. S., Winstead, E. L., True, B. S., Timko, M. T., Bhargava, A., Herndon, S. C., Miake-Lye, R. C., and Anderson, B. E.: Characterization of lubrication oil emissions from aircraft engines, Environmental science technology, 44, 9530–9534, 2010.

Zhang, C., Chen, L., Ding, S., Zhou, X., Chen, R., Zhang, X., Yu, Z., and Wang, J.: Mitigation effects of alternative aviation fuels on non-volatile particulate matter emissions from aircraft gas turbine engines: A review, Science of The Total Environment, 820, 153 233, 2022.

Zink, J., Unterstrasser, S., and Burkhardt, U.: Contrail formation for aircraft with hydrogen combustion–Part 1: A systematic microphysical investigation, EGUsphere, 2025, 1–27, 2025a.

Zink, J., Unterstrasser, S., and Jurkat-Witschas, T.: On the potential role of lubrication oil particles in contrail formation for kerosene and hydrogen combustion, Journal of Geophysical Research: Atmospheres, 130, e2025JD043 487, 2025b.

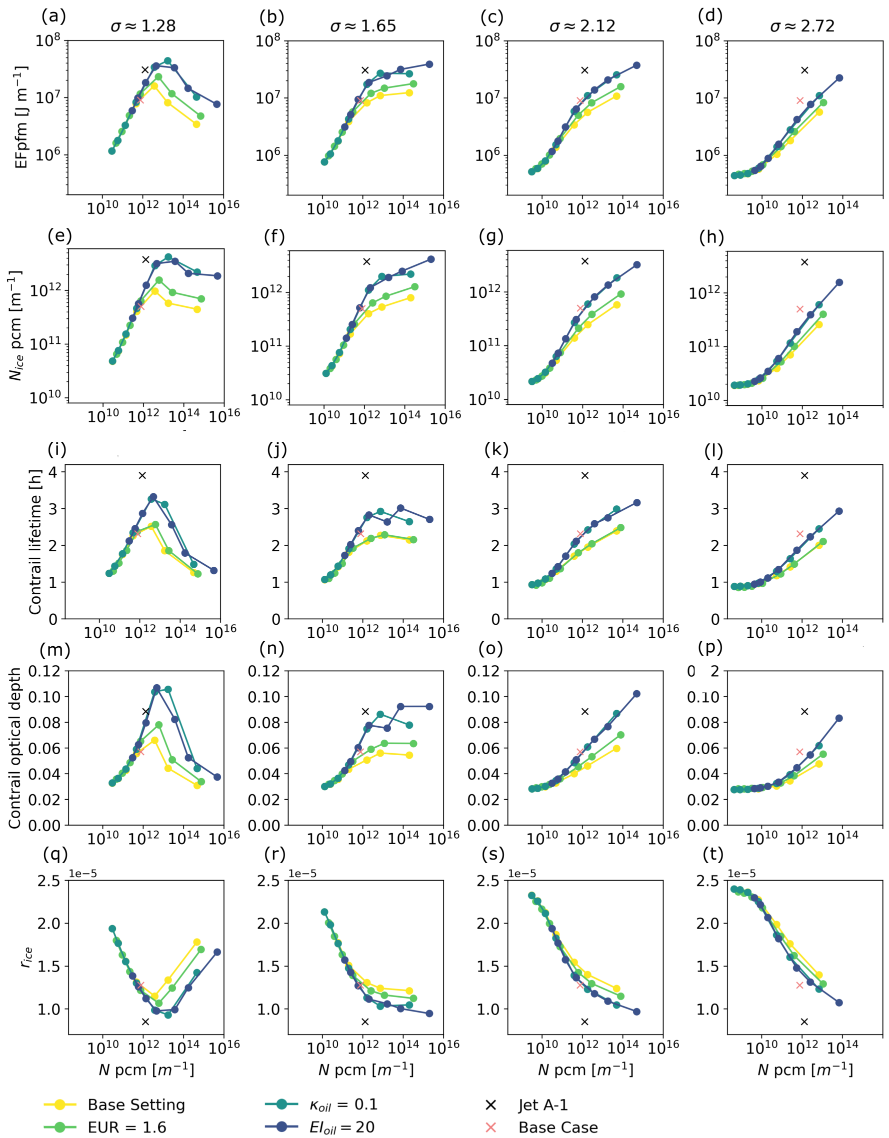

Figure 5. The figure shows the average energy forcing per flight meter (row 1), the average number of ice particles per contrail generating flight meter after downwash (row 2), the average contrail lifetime (row 3), the contrail optical depth averaged over the contrail cirrus lifetime (row 4) and the ice particle radius averaged over the contrail cirrus lifetime (row 5) for different lognormal size ~~distribution~~ distributions, geometric mean radii ~~(x-axis)~~ and ~~standard deviation~~ geometric widths (the columns) for four cases of lubrication oil parameters~~;~~. These four cases are: base setting (yellow)~~,~~; larger fuel flow for hydrogen (light green)~~,~~; large lubrication oil hygroscopicity (dark green); and high oil emission index (dark blue). The x-axes show the average number of exhaust particles per contrail generating flight meter of lubrication oil or soot, not including ambient aerosols. For comparison, the black ~~striped lines show~~ x-marker shows the average for fossil jet A-1 fuel and the pink x-marker shows the average for the base case for the same 20 randomly chosen dates. Note that the base case marker is added for comparison and has the same lubrication oil size distribution, with $\mu_o = 7.5$ nm and $\sigma_o = 1.45$ in all panels. All simulations are run for the same set of 20 randomly chosen dates.

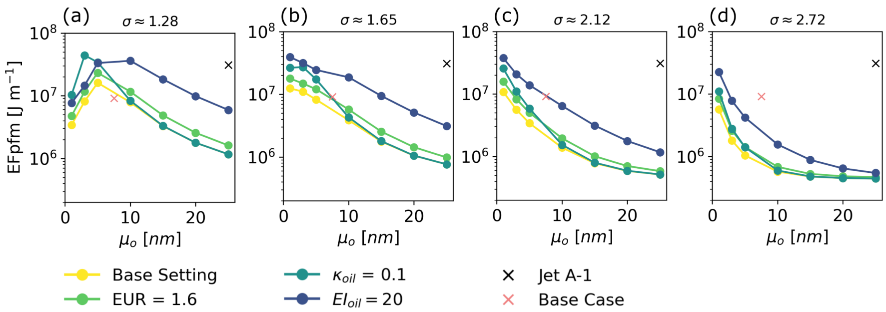

Figure 6. The figure shows the average energy forcing per flight meter for different lognormal size distributions with varying geometric mean radii (x-axis) and geometric widths (columns), for four cases of lubrication oil parameters: base setting (yellow); larger fuel flow for hydrogen (light green); large lubrication oil hygroscopicity (dark green); and high oil emission index (dark blue). For comparison, the black x-marker shows the average for fossil jet A-1 fuel (with the assumption that $\mu_s = 25$nm, as in the comparison between K15 and CoCiP's activation function). The pink x-marker shows the average for the base case described in Sec.4.1. All simulations are run for the same set of 20 randomly chosen dates.

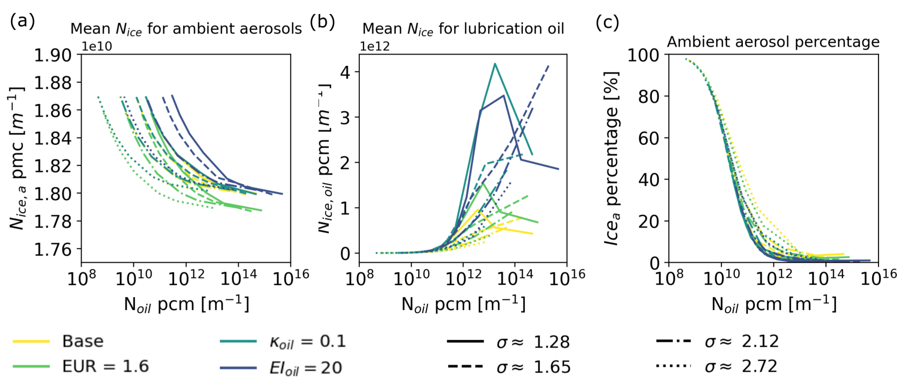

Figure 7. The figure shows the average number of ice particles after downwash per contrail flight meter stemming from ambient aerosols to the left (a) and lubrication oil in the middle (b), as well as the ambient aerosol ice ~~number~~ percentage to the right (c) for all cases as a function of the lubrication oil size distributions. Note the change of scale between panel (a) and (b).